Copper Sulfide Remobilization and Mineralization during Paleoproterozoic Retrograde Metamorphism in the Tongkuangyu Copper Deposit, North China Craton

Xuan Liu, Kuifeng Yang, Brian Rusk, Zhengjie Qiu, Fangfang Hu, Jacques Pironon

minerals

MDPI

Article

Copper Sulfide Remobilization and Mineralization during Paleoproterozoic Retrograde Metamorphism in the Tongkuangyu Copper Deposit, North China Craton

Xuan Liu [1,2,3,*], Kuifeng Yang [1], Brian Rusk [2], Zhengjie Qiu [1] and Fangfang Hu [1] and Jacques Pironon [3]

1 Key Laboratory of Mineral Resources, Institute of Geology and Geophysics, Chinese Academy of Sciences, Beijing 100029, China
2 Department of Geology, Western Washington University, Bellingham, WA 98225, USA
3 GeoRessources Lab, Université de Lorraine, CNRS, CREGU, 54500 Vandœuvre-lès-Nancy, France
* Correspondence: xuan.liu@univ-lorraine.fr; Tel.: +33-037-274-5575

Received: 6 July 2019; Accepted: 16 July 2019; Published: 18 July 2019

Abstract: The Tongkuangyu copper deposit, North China Craton, is hosted in a volcano-sedimentary sequence (ca. 2.2 Ga) that metamorphosed to the lower amphibolite facies at ca. 1.9 Ga. Petrographic observations revealed various metamorphic fabrics (mineral alignment and foliations) and several generations of biotite, chlorite, and pyrite. Sulfide Pb-Pb dating indicates that copper mineralization occurred at 1960+46/−58 Ma, younger than the zircon U-Pb age of the host metatuff (2180 Ma to 2190 Ma), but close to the timing of regional metamorphism (ca. 1.9 Ga). Electron probe analyses show that the biotites belong to the magnesium-rich variety, and were formed at 470 to 500 °C based on Ti-in-biotite thermometry. Chlorites belong to ripidolite and pycnochlorite, and were formed at ca. 350 °C based on the Al geothermometer. Pyrites in porphyry, metatuffs, and quartz veins have contrasting Ni and Co concentrations, pointing to a local remobilization. Hydrogen and oxygen isotopic analyses suggest that biotite and chlorite were formed by metamorphic waters whereas quartz records much lower δD_{fluid} values, reflecting the influence of meteoric water. Fluid inclusions in pyrite and chalcopyrite in metatuff and quartz vein contain extremely radiogenic ^{4}He and ^{40}Ar, indicating a crustal origin for the fluids. Sulfides show a magmatic sulfur isotopic signature, likely indicating the presence of preexisting volcanism-related sulfides. We proposed that the early layered copper sulfides formed during metamorphic retrogression at ca. 1.9 Ga and the late vein-type sulfides were derived from the remobilization of the earlier sulfides by infiltration of external fluids such as residual seawater and metamorphic fluids at shallow level.

Keywords: Tongkuangyu copper deposit; metamorphic fluids; Pb-Pb isochron; H-O isotopes; He-Ar isotopes

1. Introduction

The Tongkuangyu copper deposit (>3 million tonnes of copper reserves) is one of the largest copper suppliers in Northern China, and has a mining history of nearly 3400 years dating back to the Shang Dynasty [1]. Despite over six decades of research, its origin remains hotly debated. Based on the presence of porphyry, disseminated sulfides, and biotite–sericite alteration, Wang and Wen [2] inferred that it was formed by porphyry-related hydrothermal process. Xie [3] suggested that the copper mineralization was related to sedimentation and subsequent metamorphic modification based on field observations of sulfide distribution. Sun et al. [4] analyzed tourmaline in the ore-hosting sequence by

electron probe microanalysis and related their formation with the exhalation of magmatic waters under seafloor. A genetic model involving porphyry mineralization with metamorphic modification was put forward and favored on the basis of sulfur isotopes [5], H-O isotopes [6], and Re-Os geochronology [7]. A pure porphyry model was emphasized in later studies based on observations from the petrogenesis of the monzogranite porphyry [8] and fluid inclusion microthermometry [9]. Arguing against this model, Liu et al. [10,11] revealed an age gap of 60 to 70 million years between the formation of monzogranite porphyry (ca. 2180 Ma) and Mo mineralization (ca. 2120 Ma) by detailed secondary ion mass spectrometry (SIMS) and LA-ICP-MS zircon U-Pb and Re-Os dating, and discovered that the porphyry magmas had unfavorable oxygen fugacity (Δ FMQ-0.5, F: Fayalite; M: Magnetite; Q: Quartz) for porphyry mineralization. Recently, Qiu et al. [12–14] attributed Cu mineralization at Hujiayu and Henglingguan deposits in the same region to metamorphism through C-O-S isotopes, fluid inclusion, and geochronology. So far, the exact relation between Cu mineralization and metamorphism at Tongkuangyu remains elusive. In particular, the origin of the abundant biotite–chlorite alteration and source of ore-forming fluids has not been vigorously constrained. In this contribution, we present new results of U-Pb and Pb-Pb geochronology, mineral chemistry, and H-O-S-He-Ar isotopes. We proposed that the Tongkuangyu copper mineralizations are products of sulfide remobilization due to retrograde metamorphism.

2. Regional Geology

The Zhongtiao mountain is located at the southern edge of the Trans-North China Orogen (TNCO) that unifies the west and east blocks at around 1.85 Ga, forming the North China Craton [15] (Figure 1 inset). It contains Archean to Paleoproterozoic outcrops and large quantities of copper metals (>4 Mt [16]). The oldest basement of rocks, the Sushui Complex, comprises of Archean TTGs (tonalite–trondhjemite–granodiorite), early Proterozoic granitoids, and supracrustal volcanic and sedimentary rocks [17] (Figure 1), and is unconformably overlain by volcano-sedimentary rocks formed in two phases of continental rifting, known as the Jiangxian and Zhongtiao groups.

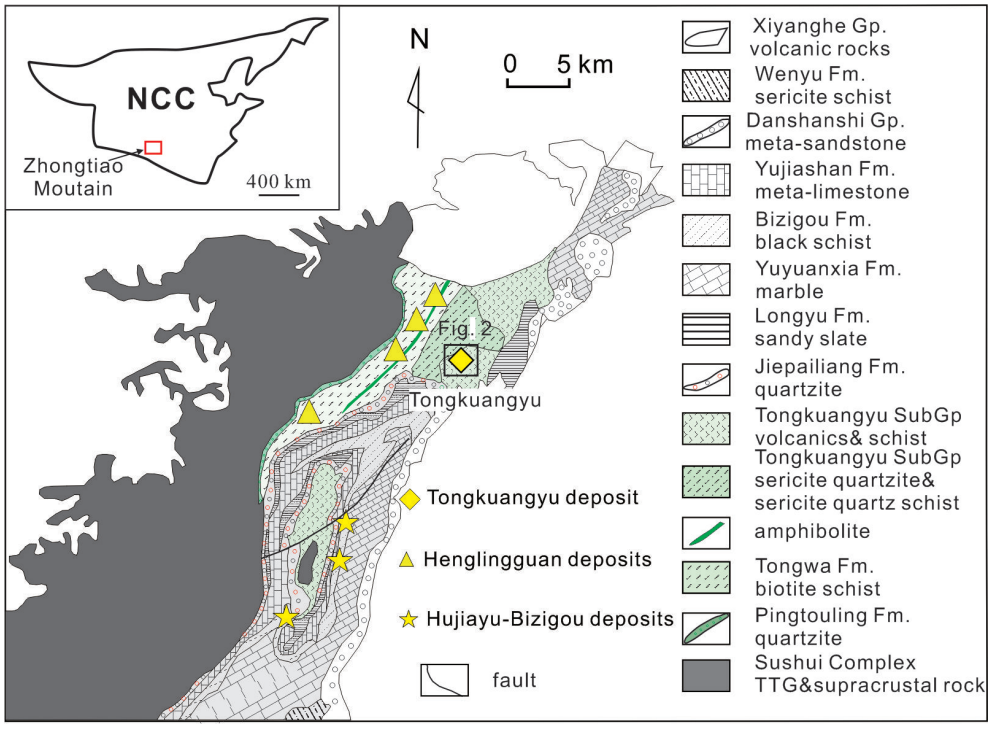

Figure 1. Geological map of the Zhongtiao mountain with an inset showing its location in the North China Craton (NCC) (adapted from Liu et al. [11]).

The Jiangxian group is divided into basal Henglingguan and upper Tongkuangyu subgroups. The Henglingguan subgroup (1000 to 1400 m thick) consists of two formations (Fm), i.e., a thin layer (around 40 m thick) of quartzite at the bottom (Pingtouling Fm), overlain by mica schists (Tongwa Fm). The Tongkuangyu subgroup (3300 m thick) is comprised of, from bottom to top, thin layers of quartzite (Houshancun Fm), quartz mica schists (Yuantoushan Fm), metamorphosed rhyolite (Shujinggou Fm), metamorphosed basic volcanic rocks (Xijinggou Fm), meta-tuff and mica schist (Luotuofeng Fm), and metamorphosed sodium-rich volcanic rocks (Songjiashan Fm) (Figure 1). The intercalated amphibolite in the Tongwa Fm yielded zircon U-Pb ages of 2.16 to 2.19 Ga determined by secondary ion mass spectrometry (SIMS) [18], and granitic intrusions and mafic volcanic rocks in the Tongkuangyu subgroup formed at 2.18 to 2.20 Ga, revealed by recent zircon geochronology studies [10,11]. A sequence of metamorphosed intermediate to basic volcanic rocks and metasediments was also exposed as inlier in the Xiyanghe group about 15 km to the east of Tongkuangyu. However, its stratigraphic relation with other rock groups are controversial. Some researchers consider it as part of the Jiangxi group, while others propose it to be part of the Zhongtiao group [19]. The Zhongtiao group (with a variable thickness between 2120 m and 8250 m) unconformably covers the Jiangxian group and is divided into six formations, from the bottom to top, of a thin layer of quarzite from the Jiepailiang Fm (150 to 200 m thick), sandy slates from the Longyu Fm, dolomitic marbles from the Yuyuanxia Fm, graphite-bearing mica schists with intercalated mafic volcanic rocks from the Bizigou Fm, metamorphosed pelitic limestones from the Yujiashan Fm, and mica schists from the Wenyu Fm [20] (Figure 1). The whole sequence is interpreted to represent a marine transgression intervened by a marine regression that led to the deposition of Bizigou Fm [5]. Zircons from the volcanic rocks in Bizigou Fm yielded U-Pb ages of 2060 to 2090 Ma [17,18], and detrital zircons from the Jiepailiang Fm yielded a maximum deposition age of ca. 2160 Ma [21]. The above rocks are unconformably overlain by greenschist-facies metamorphosed quartzite and conglomerate of the Danshanshi group (150 to 600 m thick) and unmetamorphosed andesite of the Xiyanghe group (Figure 1) during the period of 1.85 Ga [17,21]. The geologic unconformities between the Sushui and Jiangxian, Jiangxian and Zhongtiao, Zhongtiao and Danshanshi, Danshanshi and Xiyanghe groups are recognized as products of four tectonic movements, i.e., the Sushui Movement, Jiangxian Movement, and Zhongtiao Movement (Phases I and II), respectively [17]. Two major episodes of deformation have been identified in Henglingguan and Bizigou mica schists [19]. The early phase (D_1) is represented by regional foliations in the Henglingguan and penetrative axial plane schistosity of tight folds in Bizigou (S_1). The late deformation (D_2) is represented by crenulation cleavages (S_2) overprinted on S_1. Accordingly, two stages of prograde metamorphism have been distinguished and were followed by retrogression. The first prograde metamorphism occurred during D_1, and led to the gradual transformation of index mineral assemblage from chlorite-quartz-sericite through biotite-chloritoid and garnet to staurolite. The second phase of prograde metamorphism occurred during D_2, gradually forming sericite-biotite, garnet, staurolite, and kyanite. The metamorphic assemblages indicate an upper greenschist to lower amphibolite metamorphic grade. Retrogressive metamorphism is quite common and represented by the occurrence of biotite, chlorite, and sericite, replacing earlier minerals. Graphite thermometry revealed that peak metamorphism in Bizigou mica schists may have occurred at a temperature of ca. 545 °C [13]. Pressure-temperature pseudosection and mineral geothermobarometry suggested that prograde metamorphism in the Henglingguan schists occurred at temperatures of 565 °C to 630 °C. The metamorphism reached peak at temperatures of ca. 610 °C and pressures of 6.5 kbar, which was followed by a quasi-isobaric regression through temperatures of ca. 545 °C [14]. The prograde and retrograde metamorphism may have occurred at ca. 1.88 Ga and 1.86 Ga according to monazite U-Pb dating by LA-ICP-MS [14], which are consistent with monazite Th-U-Pb ages of 1.88 Ga to 1.85 Ga [22]. Copper deposits in the Zhongtiao mountain display strict lithological control and are categorized into the so-called Henglingguan, Hujiayu-Bizigou (Hu-Bi), and Tongkuangyu styles (Figure 1a). The Henglingguan style deposits are primarily hosted in the Henglingguan mica schists and amphibolite. Copper-cobalt orebodies,

parallel to schist foliation, comprise of chalcopyrite-bornite-cobaltite-pyrite lenticulars and quartz veins. Qiu et al. [14] proposed that the sulfide lenticulars formed by the enrichment of diagenetic sulfides by retrograde metamorphism, which were remobilized to form sulfide veins. The Hu-Bi style deposits are mainly hosted in the graphite-bearing mica schists, and ores comprise of early stratabound, disseminated and late vein-type sulfides. Three different models have been proposed to account for the deposit genesis, including sediment-hosted stratiform copper [23], seafloor sedimentary exhalative [4], and metamorphism-related [13]. The Tongkuangyu style deposits, represented by the Tongkuangyu copper deposit, are characterized by large and thick stratiform orebodies that are hosted within the volcano-sedimentary rocks of the Tongkuangyu subgroup. The Huping copper deposit in chlorite-amphibole schists exposed as inlier in the Xiyanghe group has recently been demonstrated as a product of three-stage metamorphic remobilization [24].

3. Deposit Geology

3.1. General Aspect

The Tongkuangyu copper deposit contains a proven reserve of three million metric tons of copper at an average grade of 0.6%. Minor economic gold, molybdenum, and cobalt are being recovered as byproducts [25]. Recent drilling has revealed a large potential of ore bodies at depths [26]. The rocks exposed in the deposit comprise of sericite quartzite, quartz mica schist and metatuff (Luotuofeng Fm), biotite schist (metamorphosed mafic volcanic rocks) (Xijinggou Fm), and meta-rhyolite (Shujinggou Fm) (Figure 2a). At depth, monzogranite porphyry intruded the metatuff. These rocks comprise of the inverted wing of a NW-dipping syncline, which belongs to a more complex regional folding system. The above rocks are crosscut by diabase and diorite dykes that are devoid of metamorphism and deformation. A total of seven ore bodies, Nos. 4 and 5 being the largest ones, exist in the deposit, which form thick slabs parallel to the foliations of the host rocks (Figure 2b,c). The ore bodies are primarily hosted in the metatuff (Figure 2c), being comprised of two types of mineralization, i.e., the early layered sulfides, and the late quartz veins (Figure 2d; Figure 3j,k). Metal sulfides in the mineralized layers mainly include chalcopyrite and pyrite, intergrowing with biotite, albite, and quartz. Sulfides in the veins include chalcopyrite, pyrite, bornite, molybdenite, and minor amounts of chalcocite, intergrowing with chlorite, sericite, muscovite, rutile, clausthalite, hematite, and magnetite.

3.2. Metamorphic and Alteration Petrography

At Tongkuangyu, various metamorphic fabrics and mineral assemblages are present. Mineral alignment and foliation is commonly observed in metatuff (Figure 3a), meta-porphyries (Figure 3b), and mica quartz schist (Figure 3c). In the metatuff and metaporphyry, quartz is elongated and displays undulatory extinction and subgrain recrystallization (Figure 3d,e), explicitly suggesting that the host rocks and layered mineralizations were affected by deformation. By contrast, the vein quartz is devoid of a recrystallization texture and undulatory extinction, signaling limited influence by deformation (Figure 3f).

Minerals formed during prograde and peak metamorphism are poorly preserved in the deposit area compared to rocks in Henglingguan due to strong retrogression. Only in some meta-mafic volcanic rocks, sillimanite (Figure 3g), and relict garnet were observed with muscovite, biotite and minor amounts of quartz, tourmaline, and rutile. Some mica schists contain relicts of porphyroblastic scapolite (Figure 3h,i), which are commonly replaced by sericite, biotite, chlorite, quartz, and apatite (Figure 3i). These characteristic minerals are absent from mica schist, granodiorite porphyry, and metatuff. In these rocks, however, metamorphic assemblages are characterized by oriented sericite, muscovite, biotite, pyrite, and hematite or discontinuous segregations of quartz, albite, and dolomite (Figure 3a–e). The sillimanite - scapolite - biotite - muscovite in mafic volcanic rocks and albite - quartz - biotite - sericite - rutile in felsic rocks are interpreted as the earliest metamorphic assemblages, which are designated as Stage I. The minerals of metamorphic assemblage are pervasively overprinted by biotite,

muscovite, sericite, quartz, chlorite, apatite, tourmaline, hematite, chalcopyrite, magnetite, pyrite, and bornite. These minerals might have been derived from retrograde metamorphism with the presence of fluids (termed as Stage II). Foliation-parallel chalcopyrite and chalcopyrite-bearing leucosomes contribute the most to the total reserves (Figure 3a,j). Metamorphosed rocks, metatuff in particular, are commonly crosscut by (magnetite-bornite-chalcopyrite) hematite quartz veins. The veins, several to several tens of centimeters wide, have irregular vein boundaries and are brecciated (Figure 3k) and cemented by chalcopyrite, bornite, and magnetite (Figure 3i). The hematite and quartz likely formed at Stage II, whereas the cementing minerals may have been formed at a later stage.

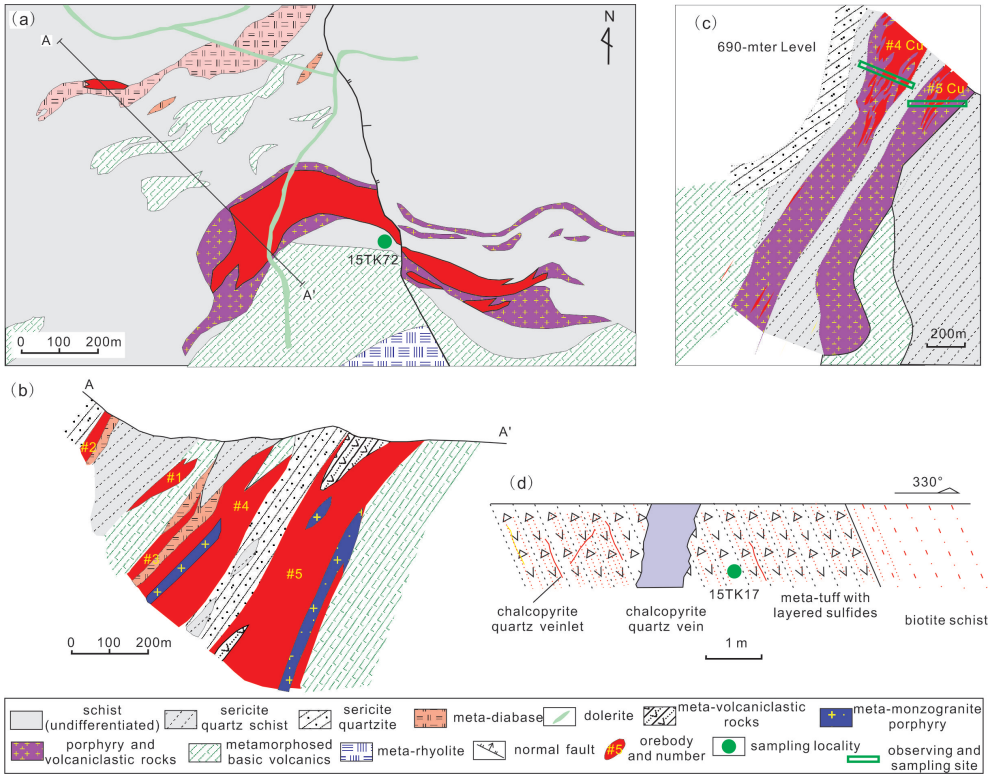

Figure 2. (**a**) Geologic map of the Tongkuangyu copper deposit showing primary lithologies, structure, and ore bodies; (**b**) A to A′ cross section showing the attitudes of the ore-hosting rocks and ore bodies; (**c**) A plenary geological map of the underground working at the level of 690 m with locations for observing and sampling; and (**d**) A field sketch of the underground tunnel at the level of 554 m with locations for observing and sampling.

The latest veins (termed as Stage III), crosscutting the hematite quartz vein, consist of quartz, chlorite, chalcopyrite, magnetite, and rutile (Figure 3m). In the hematite mica schists, veinlets of hematite/magnetite intergrow and chalcopyrite/bornite have been observed [10]. They constitute a significant proportion of the Cu ores. This mineral assemblage can also occur as disseminations, and normally replaces preexisting biotite. The replacement leads to the formation of biotite pseudomorphs of chalcopyrite, magnetite, and chlorite (Figure 3n–o). A graphic illustration of mineral paragenesis is given in Figure 4, and a more detailed description of the petrography can be found in Liu et al. [10].

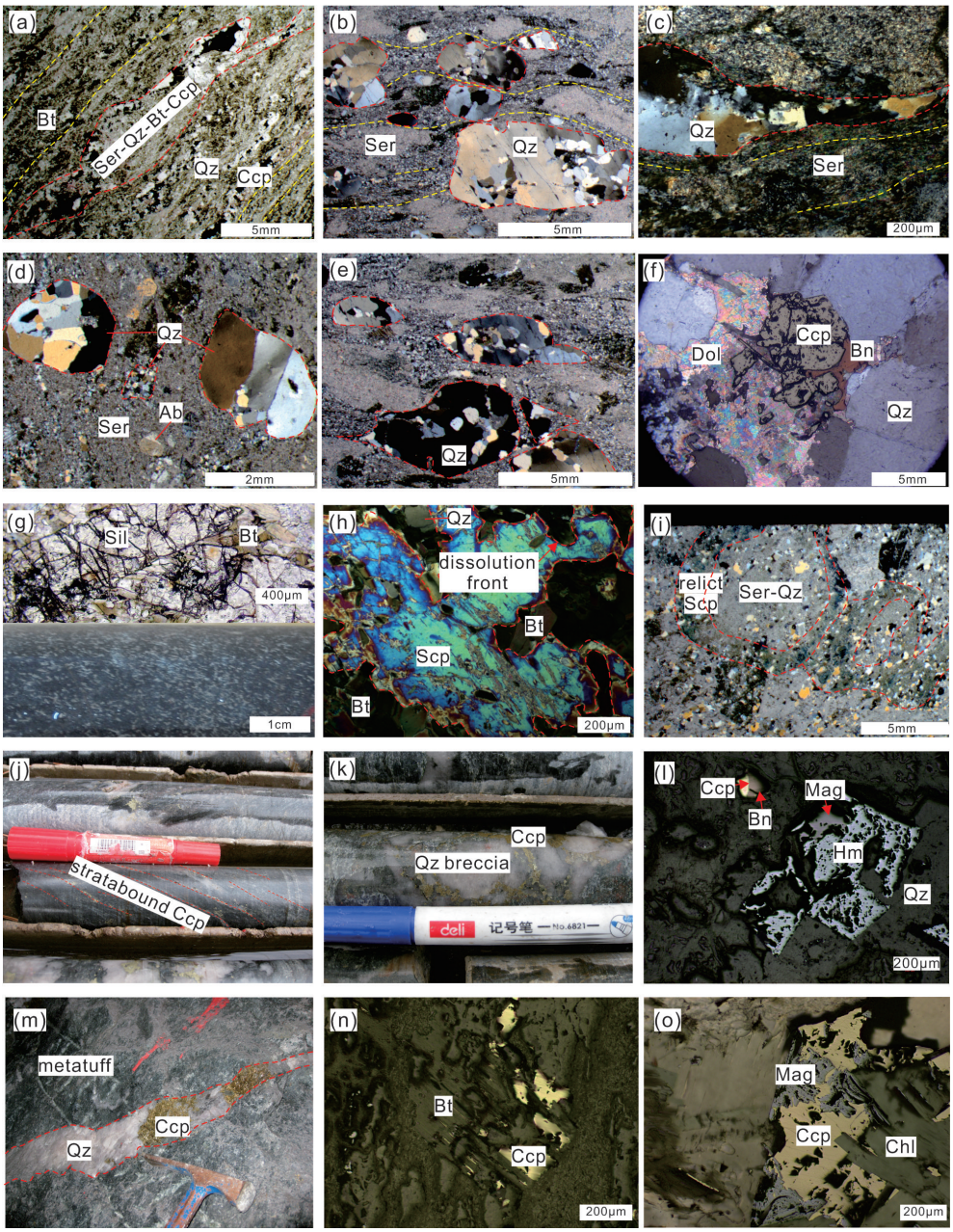

Figure 3. Petrographic and field photos of the Tongkuangyu copper deposit. (**a**) Mineral alignments in metatuff with biotite thin layers and sericite-quartz-biotite-chalcopyrite thick layers; (**b**) Mineral alignments in monzogranite porphyry with sericite layers and deformed quartz aggregates; (**c**) Mineral alignments of sericite and quartz-(albite) lenticulars; phenocrystic quartz in metatuff (**d**) and monzogranite porphyry (**e**) exhibits undulatory extinction and subgrain recrystallization; (**f**) Quartz from the hematite-quartz vein shows no sign of influence by ductile deformation; (**g**) Sillimanite and biotite in the mafic volcanic rocks; (**h**,**i**) Scapolite in the mica schist, which was dissolved by biotite, sericite, and quartz; (**j**) Layered chalcopyrite mineralization in metatuff; (**k**,**l**) Chalcopyrite-quartz veins in the metatuff; (**m**) Chalcopyrite and chlorite replacing preexisting biotite in metatuff under cross-polarized (**m**) and reflected light (**n**); (**o**) Chalcopyrite and chlorite replacing preexisting biotite in biotite schist. Ab: Albite; Bn: Bornite; Bt: Biotite; Ccp: Chalcopyrite; Dol: Dolomite; Hm: Hematite; Mag: Magnetite; Qz: Quartz; Scp: Scapolite; Ser: Sericite; Sil: Sillimanite.

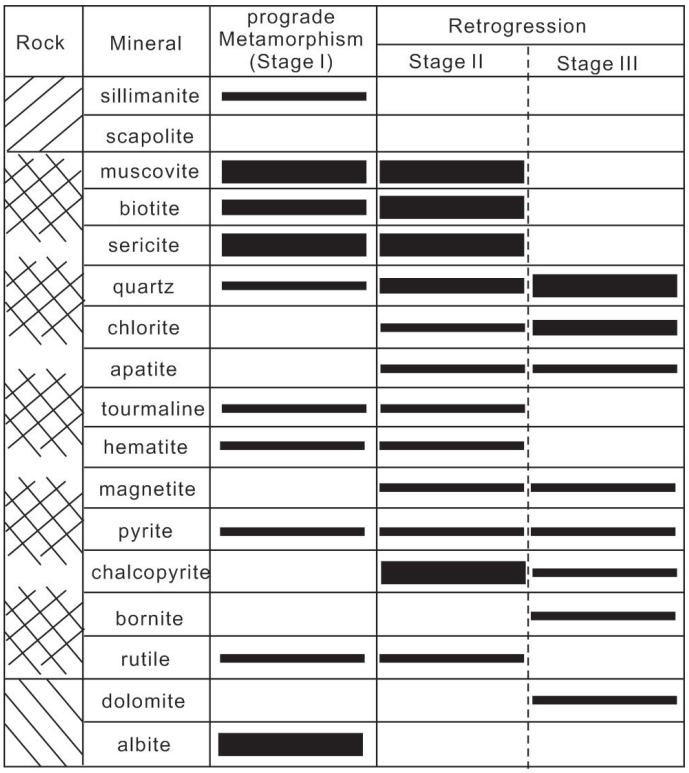

Figure 4. Mineral sequences occurred during peak and retrograde metamorphism at the Tongkuangyu copper deposit, North China Craton. Note that sillimanite and scapolite are only present in the mafic rocks (denoted by slash lines in the first column), albite and dolomite are only present in felsic rocks (denoted by reverse slash lines in the first column), and all other minerals are present in both lithologies. The thickness of the bars represents the relative amount of mineral in each stage.

4. Materials and Methods

The rock samples were collected from underground workings (Levels 690 m and 540 m), outcrops and drill cores (NOs. 4S044, 4S046, 4S047, 4S048, and 4S126). Thin sections were made for petrographic observation and electron microprobe analysis. Mineral separates (purity >90%) were acquired by conventional magnetic and gravitational methods followed by hand picking.

4.1. Zircon U-Pb Dating

Selected zircons were mounted in epoxy, ground, and polished to obtain good surfaces. The mounted grains were imaged by reflected and transmitted lights with a conventional microscope and by cathodoluminescence (CL) with a Nova NanoSEM field emission scanning electron microscope equipped with a Gatan MonoCL4 detector at the Institute of Geology and Geophysics, Chinese Academy of Sciences (IGGCAS). Zircon U-Pb dating was performed on a Thermo iCAP Qc ICP-MS instrument attached with a RESOlution-S155 ArF Excimer 193 nm laser system at the Division of Geochemistry of the State Key Laboratory of Geological Processes and Mineral Resources, China University of Geosciences, Wuhan. Argon was used as the makeup gas and mixed with the carrier gas (helium) via a T-connector. A diameter of 33 μm and a repetition rate of 10 Hz was used. Nitrogen was added into the central gas flow (Ar+He) of the Ar plasma to decrease the detection limit and improve sensitivity. Each analysis incorporated a background acquisition of approximately 20 to 30 s (gas blank) followed by 30 s data acquisition from the sample. Zircon 91500 [27] was used as external standard and was analyzed twice every 5 analyses. Zircon standard Plešovice [28] was used for monitoring data quality. Uncertainty of preferred values for the external standard 91500 was propagated to the ultimate results of the samples. Off-line selection and integration of background and analytical signals, and time-drift correction and quantitative calibration for U-Pb dating were

performed by ICPMSDataCal [29]. Concordia diagrams and weighted mean calculations were made using Isoplot [30].

4.2. Electron Probe Microanalysis

Major elements of biotite, chlorite, pyrite, chalcopyrite, and bornite were obtained on JEOL JXA-8100 electron microprobe with wavelength-dispersive spectroscopy (WDS) at IGGCAS. Data on SiO_2, TiO_2, Al_2O_3, FeO, MnO, MgO, CaO, Na_2O, K_2O, F, and Cl were collected for gauge minerals, and Se, As, S, Fe, Cu, Co, Pb, Ni, Ag, Te, Zn, and Au for sulfides. During analysis, an accelerating voltage of 15 kV was used to generate a focused electron beam of 5 µm in diameter and 10 nA of current. Natural minerals (K-feldspar, kaersutite, bustamite, garnet, diopside, olivine, and apatite) were used as standards. The ZAF correction method was used to correct the atomic number (Z), absorption (A), and fluorescence (F) effect for all analyzed minerals.

4.3. H-O-S-Pb Isotopes

Hydrogen, oxygen, sulfur, and lead isotopes of mineral separates were acquired at the Analytical Laboratory of the Beijing Research Institute of Uranium Geology (BRIUG). To obtain oxygen isotopes in biotite, chlorite, and quartz, the mineral separates were reacted with pure BrF5 at 500 °C to 680 °C for 14 h. The released gas mixtures were purified for oxygen gases, which were reacted with graphite to produce CO_2 under a temperature of 700 °C with the presence of catalyzing Pt. The CO_2 was then sent into a MAT253 mass spectrometry for determination of oxygen isotopes (^{18}O and ^{16}O). The reported results were normalized to the standard Vienna Standard Mean Ocean Water (VSMOW) in a notion of $\delta^{18}O_{qtz}$. The analytical precision was better than ±0.2%. For hydrogen isotopes of quartz, the mineral separates were decrepitated within a ceramic tube with the presence of graphite, and the released gas mixtures were then reacted with graphite to produce H_2 which was carried to the mass spectrometry for analysis. For hydrogen isotopes of biotite and chlorite, about 2 mg separated was dried at 100 °C for 1 h, and then was combusted at 1450 °C in a graphite crucible to convert the hydroxyls into H_2 which was carried to a MAT253 mass spectrometry for analysis. The results were normalized with respect to VSMOW, and are reported as δD (permil). The analytical precision was better than ±1 %. Sulfur isotopic ratios were acquired on a MAT-251 mass spectrometer at BRIUG. Sulfide separates (40 to 60 mesh) were mixed with cuprous oxides and were crushed into 200 mesh powders. The sulfide was converted into SO_2 gases by the oxidation reaction with the cuprous oxides at 980 °C under a vacuum atmosphere (2×10^{-2} Pa). ^{34}S and ^{32}S of SO_2 were then determined by the mass spectrometer. Results were reported in $\delta^{34}S$ (per mil) with respect to Vienna Canyon Dioblo Troilite (V-CDT). Analytical precisions were better than ±0.2%. Lead isotopic compositions of sulfide were obtained on a MAT261 mass spectrometry at BRIUG. About 100 mg of sulfide separates were dissolved in with a mixture of HF and perchloric acids, which was then dried. The remaining solids were re-dissolved by HCl and dissolved again by 0.5N HBr to separate Pb. The solutions were loaded into anion-exchange resin, and then leached sequentially by 0.5N HBr, 2N HCl, and 6N HCl to separate Pb. After being dried, the Pb-bearing solids were analyzed by an Isoprobe-T mass spectrometry. Measured isotopic values for NBS981 were $^{208}Pb/^{204}Pb$: 2.165247 ± 0.000069, $^{207}Pb/^{204}Pb$: 0.914510 ± 0.000056, $^{206}Pb/^{204}Pb$: 0.059200 ± 0.00013. Errors are reported in 2σ. Background Pb content for the analysis was 0.1 ng.

4.4. He-Ar Isotopes

Helium and argon isotopes of fluid inclusions in pyrite and chalcopyrite separates were obtained at IGGCAS. Detailed descriptions about analytical equipment and procedures is available in He et al. [31]. Sulfide separates were loaded into an aluminum holder, and then were crushed by applying a hydraulic press to the piston at a room temperature of 20 °C. Gases were released by in-vacuo one-step crushing at about 2000 psi pressure, which was capable of minimizing contribution from lattice-hosted and atmospheric gas components. The released gases were purified with one cold finger at liquid N_2 and four SAES Zr-Al getters (two at 20 °C, the other two at 450 °C). Argon was

adsorbed on charcoal in a cold finger at liquid nitrogen temperature, and then helium was trapped on charcoal at a temperature of 10 K by a cyropump. Isotopic determinations were performed on a Noblesse mass spectrometer operating in static mode. A cold GP50 getter and liquid nitrogen-cooled charcoal trap were used to minimize the partial pressure of residual gases during analysis. ^{3}He was measured in pulse-counting mode using the central electron multiplier while ^{4}He was measured on a Faraday cup. ^{36}Ar, ^{38}Ar, and ^{40}Ar were simultaneously measured on three multipliers. The standard air was measured every two weeks, which had ^{3}He/^{4}He ratio was 1.4×10^{6} and ^{40}Ar/^{36}Ar ratio for air was measured at 345.1. The uncertainty of average ^{3}He/^{4}He ratio was better than 5%. The measured results of samples were normalized to the standard air and corrected for system blanks. After crushing, the remaining samples were passed through a 100 mesh sieve and weighed (typically <40% of the sample was crushed to <75 μm). The reported noble gas concentrations in minerals were calculated assuming that the only gas to be extracted was from the <75 μm fraction, and that all the gas was extracted from this size fraction [32].

5. Results

5.1. Geochronology

While formation ages of the meta-monzogranitic porphyry have been well constrained by laser ablation ICPMS and secondary ion mass spectrometry (SIMS) (2180 Ma to 2190 Ma, Liu et al. [10,11]), the formation timing of the metatuff and copper mineralization remains poorly defined. Existing results yielded a large range of age from 2115 Ma to 2200 Ma for the metatuff (see a compilation in Liu et al., [10]). The mineralization age is largely constrained by two molybdenite Re-Os studies (ca. 2110 Ma [7,10]). However if this age represents the age of major Cu mineralizing events are still under debate as the relations between the molybdenite and sulfides of Stage II and Stage III are unclear.

5.1.1. Zircon U-Pb Dating

Zircon grains separated from metatuff collected from the eastern outcrop (15TK72) are euhedral. Under CL, most of the zircons show oscillatory zoning with several grains exhibiting bright homogeneous cores and dark rims (Figure 5a). A total of 23 spots were analyzed by LA-ICP-MS. They show wide ranges in ^{206}Pb/^{238}U and ^{207}Pb/^{235}U, and form a discordia intercepting with the concordia at 2137 ± 19 Ma with large scatter (MSWD = 4.8) (Figure 5b). On the discordia, seven data points plot above the concordia while 13 points plot below the concordia, which likely result from the preferential loss of U and Pb, respectively [33]. The scatter likely results from multiple episodes of open-system behavior [33]. The interpretation is supported by the observation that the above-concordia analyses have higher Pb/U ratios while the below-concordia ones have lower Pb/U ratios compared to the concordant ones (Figure 5c). Besides, the above-concordia zircon was brighter than the concordant ones possibly due to a reduced content of U. Therefore, the concordant analyses (♯8 and ♯13; Table 1) was considered more reliable than the disconcordant intercept age. The former yielded an averaged ^{206}Pb/^{238}U age of 2181 ± 2.2 Ma (1σ).

By contrast, zircon crystals from the rock sample collected in the underground tunnel were rounded in shape. Under CL, a range of features were observed (Figure 5a). Although those grains with oscillatory zoning were selected for dating, a large range of concordant ages were extracted. Overall, 10 out of 23 analyzed spots are concordant (concordance >98%), but yield a wide spectrum of ^{206}Pb/^{238}U ages ranging from 2178 Ma to 3405 Ma (Figure 5d; Table 1), which is comparable to detrital zircons in the Tongkuangyu subgroup [21]. Therefore, the minimum age of 2178 ± 30.7 Ma (1σ) might represent the age of this sample, which was formed contemporaneously with the porphyry and mafic volcanic rocks [10,11].

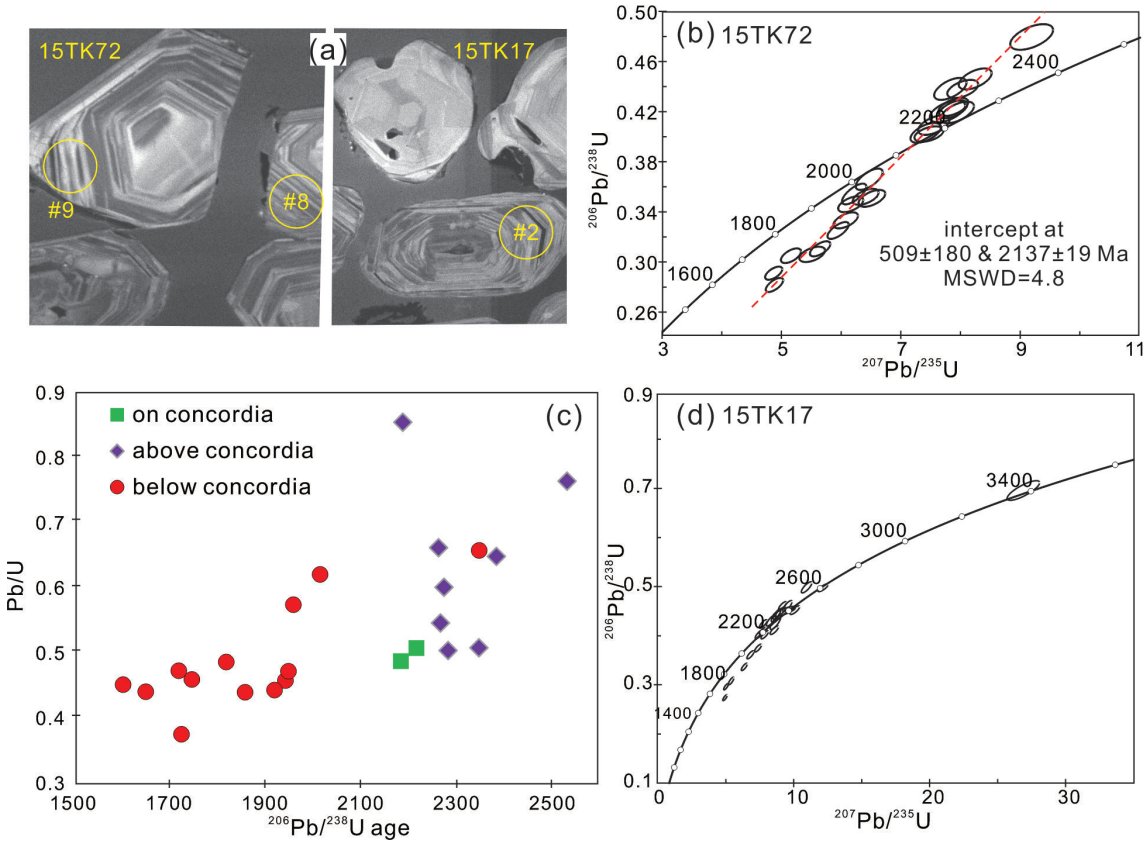

Figure 5. (**a**) Cathodoluminescence images for zircon of metatuff of the Tongkuangyu Cu deposit, North China Craton; (**b**,**d**) U-Pb concordia diagrams for 15TK72 and 15TK17; and (**c**) A plot of ^{206}Pb/^{238}U versus Pb/U for 15TK72.

5.1.2. Sulfide Pb-Pb Dating

Lead isotopes of sulfide (pyrite, chalcopyrite) from sulfide quartz veins and quartz biotite schist were also analyzed. Results show that they have extremely radiogenic Pb isotopic compositions (^{206}Pb/^{204}Pb: 26.7 to 108.6, ^{207}207Pb/^{204}Pb: 16.6 to 26.2, ^{208}Pb/^{204}Pb: 43.0 to 79.5) (Figure 6a,b; Table 2). On a ^{207}Pb/^{204}Pb-^{206}Pb/^{204}Pb diagram, these data plot well above all known lead reservoirs and yield a well-fit linear array (Figure 6a). A linear regression by Isoplot [30] yields a slope corresponding to an age of 1912+160/−150 Ma. Compared to previous data [34], this study revealed much higher Pb ratios, but they plot along the same linear trend. It is also noted that lead isotopes of sulfide from Hu-Bi and Henglingguan copper deposits plot along this linear array, yielding an identical age with smaller uncertainties (1964+46/−58 Ma) (Figure 6c). Compared to major Pb reservoirs (Figure 6d), ^{206}Pb/^{204}Pb and ^{207}207Pb/^{204}Pb ratios in sulfides of the Zhongtiao mountain are higher than those of the upper crust and comparable to Mississippi Valley-type deposits.

Table 1. Results of zircon U-Pb dating on Tongkuangyu monzogranitic porphyries, Zhongtiao mountain, North China Craton.

	Th	U	$^{207}Pb/^{206}Pb$	1σ	$^{207}Pb/^{235}U$	1σ	$^{206}Pb/^{238}U$	1σ	$^{207}Pb/^{206}Pb$	1σ	$^{207}Pb/^{235}U$	1σ	$^{206}Pb/^{238}U$	1σ	Continued
	ppm	ppm	Ratio		Ratio		Ratio		Age (Ma)		Age (Ma)		Age (Ma)		
15TK72-1	160	464	0.132596	0.003564	6.507720	0.182921	0.350795	0.005490	2132	52	2047	25	1938	26	94%
15TK72-2	220	512	0.129750	0.003308	6.403430	0.176909	0.352037	0.005217	2095	44	2033	24	1944	25	95%
15TK72-3	77.9	123	0.135365	0.003510	7.937943	0.228860	0.419388	0.007038	2169	45	2224	26	2258	32	98%
15TK72-4	94.6	319	0.132544	0.003098	7.870702	0.204647	0.423792	0.005930	2132	41	2216	23	2278	27	97%
15TK72-5	224	468	0.131296	0.003076	5.941478	0.145733	0.325153	0.005513	2117	46	1967	21	1815	27	91%
15TK72-6	132	260	0.133746	0.003104	7.869795	0.193886	0.421906	0.005832	2148	41	2216	22	2269	26	97%
15TK72-7	314	566	0.130290	0.002858	5.639331	0.140118	0.310505	0.004931	2102	39	1922	21	1743	24	90%
15TK72-8	126	343	0.131646	0.003249	7.408248	0.208270	0.403092	0.006465	2120	43	2162	25	2183	30	99%
15TK72-9	225	519	0.130358	0.003080	6.068570	0.167968	0.333227	0.005233	2103	41	1986	24	1854	25	93%
15TK72-10	125	252	0.132539	0.003509	7.773304	0.241875	0.420249	0.007076	2132	46	2205	28	2262	32	97%
15TK72-11	93.5	142	0.137270	0.003834	9.184007	0.293271	0.479612	0.008367	2194	50	2357	29	2526	36	93%
15TK72-12	116	317	0.129485	0.003851	5.507699	0.175762	0.306076	0.004994	2091	52	1902	27	1721	25	90%
15TK72-13	131	394	0.133465	0.003393	7.464090	0.199285	0.402146	0.005006	2144	44	2169	24	2179	23	99%
15TK72-14	202	525	0.127731	0.003130	6.152720	0.171515	0.346059	0.005146	2078	38	1998	24	1916	25	95%
15TK72-15	67.3	227	0.131839	0.003163	8.029580	0.212421	0.438105	0.005927	2124	42	2234	24	2342	27	95%
15TK72-16	88.6	158	0.133080	0.003169	8.238265	0.225389	0.446136	0.006850	2139	41	2258	25	2378	31	94%
15TK72-17	173	227	0.126858	0.002816	6.210369	0.166735	0.354270	0.006768	2055	39	2006	24	1955	32	97%
15TK72-18	101	94.3	0.133026	0.003215	7.544670	0.215092	0.409258	0.006355	2139	42	2178	26	2212	29	98%
15TK72-19	502	689	0.125083	0.002520	4.874860	0.119185	0.281679	0.004591	2031	35	1798	21	1600	23	88%
15TK72-20	66.1	115	0.129282	0.003252	7.821594	0.221500	0.438180	0.007175	2088	44	2211	26	2342	32	94%
15TK72-21	421	695	0.120703	0.002398	4.861564	0.117308	0.291056	0.004287	1966	35	1796	20	1647	21	91%
15TK72-22	225	313	0.127552	0.002724	6.462004	0.184302	0.366062	0.006952	2065	37	2041	25	2011	33	98%
15TK72-23	259	487	0.122368	0.002789	5.151616	0.137893	0.304989	0.004782	1991	41	1845	23	1716	24	92%
15TK17-1	103	174	0.138998	0.003799	8.332893	0.283288	0.431033	0.009173	2215	48	2268	31	2310	41	98%
15TK17-2	450	832	0.121614	0.002785	5.015080	0.139951	0.296264	0.005185	1980	41	1822	24	1673	26	91%
15TK17-3	30.5	1018	0.129512	0.002797	4.940881	0.134594	0.273926	0.004877	2091	38	1809	23	1561	25	85%
15TK17-4	278	887	0.125591	0.002829	5.394423	0.164264	0.308019	0.006340	2039	39	1884	26	1731	31	91%
15TK17-5	220	380	0.142210	0.003187	8.767293	0.233089	0.444142	0.008589	2254	38	2314	24	2369	38	97%
15TK17-6	228	242	0.157593	0.003776	10.944491	0.315616	0.498572	0.009218	2431	41	2518	27	2608	40	96%
15TK17-7	150	224	0.141281	0.003288	8.670424	0.266669	0.439483	0.008994	2243	41	2304	28	2348	40	98%
15TK17-8	186	554	0.135390	0.003146	6.361816	0.181396	0.336660	0.006125	2169	40	2027	25	1871	30	91%
15TK17-9	95.5	93.8	0.132500	0.003657	7.463651	0.243966	0.403018	0.007400	2131	53	2169	29	2183	34	99%

Table 1. *Cont.*

	Th	U	$^{207}Pb/^{206}Pb$	1σ	$^{207}Pb/^{235}U$	1σ	$^{206}Pb/^{238}U$	1σ	$^{207}Pb/^{206}Pb$	1σ	$^{207}Pb/^{235}U$	1σ	$^{206}Pb/^{238}U$	1σ	Continued
	ppm	ppm	Ratio		Ratio		Ratio		Age (Ma)		Age (Ma)		Age (Ma)		
15TK17-10	118	279	0.130789	0.003541	7.756137	0.238536	0.424231	0.007001	2109	47	2203	28	2280	32	96%
15TK17-11	157	318	0.276175	0.007738	26.897195	0.978275	0.695829	0.016311	3342	44	3380	36	3405	62	99%
15TK17-12	158	265	0.144044	0.004309	9.028967	0.296604	0.448769	0.007918	2276	52	2341	30	2390	35	97%
15TK17-13	131	206	0.145893	0.004750	8.654297	0.318667	0.426837	0.011423	2298	55	2302	34	2291	52	99%
15TK17-14	252	415	0.159669	0.004192	10.081618	0.290057	0.452187	0.007142	2454	44	2442	27	2405	32	98%
15TK17-15	256	493	0.149101	0.003783	8.569544	0.253865	0.411300	0.007007	2336	49	2293	27	2221	32	96%
15TK17-16	305	441	0.140788	0.003299	7.375779	0.206542	0.374953	0.006400	2237	40	2158	25	2053	30	94%
15TK17-17	223	384	0.134921	0.003142	7.710761	0.195892	0.409955	0.005692	2165	40	2198	23	2215	26	99%
15TK17-18	150	281	0.142554	0.003211	9.171776	0.237656	0.461026	0.006915	2258	39	2355	24	2444	31	96%
15TK17-19	144	197	0.148710	0.003841	9.530019	0.282890	0.460601	0.009029	2331	44	2390	27	2442	40	97%
15TK17-20	114	135	0.135560	0.003963	6.816048	0.215324	0.361343	0.006744	2172	50	2088	28	1989	32	95%
15TK17-21	179	221	0.175285	0.004039	12.155594	0.302240	0.497735	0.006440	2609	38	2616	23	2604	28	99%
15TK17-22	130	186	0.149743	0.011119	9.315985	0.676213	0.449482	0.008341	2343	127	2370	67	2393	37	99%
15TK17-23	142	228	0.140824	0.003670	7.865361	0.226347	0.401870	0.006669	2239	46	2216	26	2178	31	98%

Table 2. Pb isotopic composition of sulfides of the Tongkuangyu Cu deposit, North China Craton.

Sample No.	Host Rock	Mineral	$^{208}Pb/^{204}Pb$	sd	$^{207}Pb/^{204}Pb$	sd	$^{206}Pb/^{204}Pb$	sd
13TK30	Metamorphosed tuff	Chalcopyrite	79.49	0.031	26.2	0.01	108.6	0.041
13TK44	Chalcopyrite quartz vein	Chalcopyrite	65.41	0.016	20.5	0.005	58.77	0.014
13TK62-1	Chalcopyrite quartz vein	Chalcopyrite	76.05	0.025	21.4	0.008	64.19	0.021
13TK67	Breciated quartz vein cemented by chalcopyrite	Chalcopyrite	43.00	0.009	16.6	0.004	26.65	0.007
13TK74	Breciated quartz vein cemented by chalcopyrite	Chalcopyrite	74.67	0.018	20.9	0.005	60.35	0.014
13TK89	Biotite schist with sulfide disseminates	Pyrite	73.02	0.025	21.5	0.007	66.23	0.021
13TK90	Chalcopyrite quartz vein	Chalcopyrite	66.10	0.019	18.9	0.005	43.32	0.013

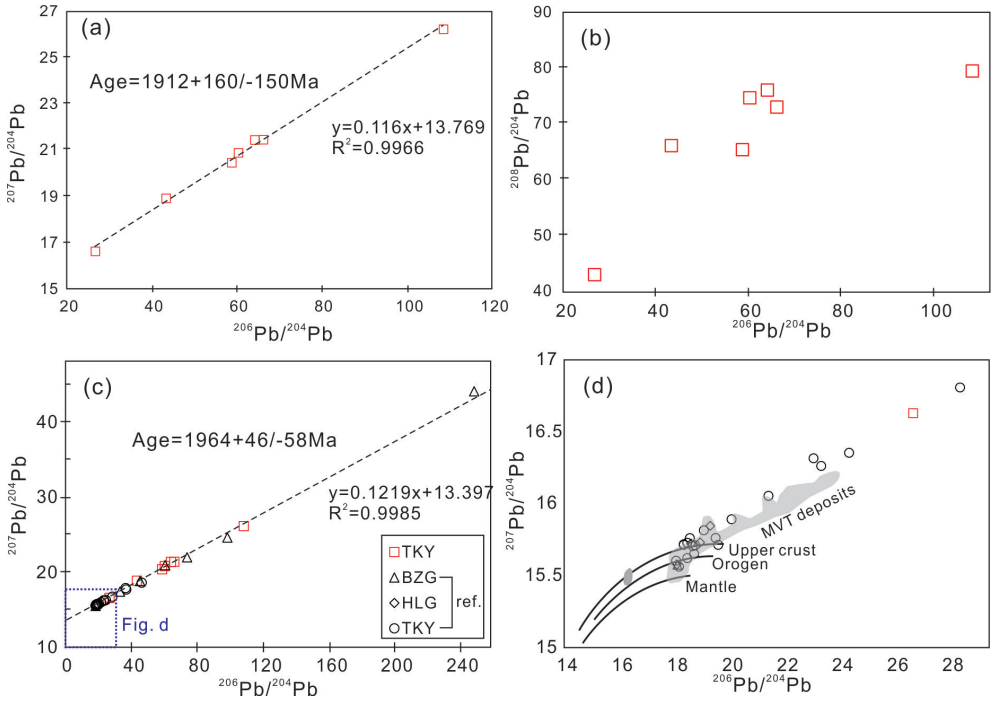

Figure 6. (**a**,**b**) Plots of $^{206}Pb/^{204}Pb$ versus $^{207}207Pb/^{204}Pb$ and $^{208}Pb/^{204}Pb$ versus $^{206}Pb/^{204}Pb$ of sulfides of the Tongkuangyu Cu deposits, North China Craton; (**c**) A plot of $^{206}Pb/^{204}Pb$ versus $^{207}Pb/^{204}Pb$ with previous data of Tongkuangyu, Bizigou and Henglingguan; (**d**) A comparison between Zhongtiao mountain and other Pb reservoirs (adapted from [35,36]).

5.2. Mineral Chemistry

5.2.1. Biotite

Biotites of Tongkuangyu were formed during metamorphism and retro-grade metasomatism. Those that occur co-oriented with peak metamorphic minerals are products of prograde metamorphism (Stage I). This type of biotite was observed in the biotite schist (named as Bt I_{BS}) (Figure 7a) and deformed porphyry (termed as Bt I_{DP}) (Figure 7b). Non-oriented biotites that crosscut and rim the early metamorphic minerals are products of retrogression (Stage II), including those biotite vein in porphyry (Bt II_{VP}) (Figure 7c), biotite phenocrystic pseudomorph in porphyry (Bt II_{PP}) (Figure 7d), biotite vein in metatuff (Bt II_{VT}) (Figure 7e), biotite surrounding and crosscutting quartz-albite segregations in metatuff (Bt II_{CT}), and biotite in quartz albite segregations that were overprinted by late chalcopyrite-pyrite-chlorite mineralization (Bt II_{SM}) (Figure 7f). "Bt" in the abbreviation represent biotite, "I" and "II" correspond to Stage I and II, and the subscript represent the type of host rock.

Electron probe microanalysis (EPMA) and calculation on the basis of 11 oxygen atoms reflects that all types of biotite have consistently high Al (1.38–1.77 apfu), Mg (1.08–1.63 apfu), and Ti (0.05–0.11 apfu), and have low K_2O (0.7–1.01 apfu) and Fe (0.75–1.21 apfu) (Table S1). Most of these biotites belong to magnesium-rich biotite on the $Mg - (Al^{VI} + Fe^{3+} + Ti) - (Fe^{2+} + Mn)$ ternary diagram (Figure 8a). On a molar Mg/(Mg + Fe) versus Cl plot (Figure 8b), Bt I_{BS} is characterized by high Cl contents but low Mg/(Mg + Fe) values; Bt I_{DP} and Bt II_{VP} occupy the low Mg/(Mg + Fe) and Cl region; Bt II_{VT} and Bt II_{CT} form a smooth trend from a Cl-rich component to a Mg/(Mg + Fe) high component; and Bt II_{SM} is characterized by low Cl but high Mg/(Mg + Fe) values.

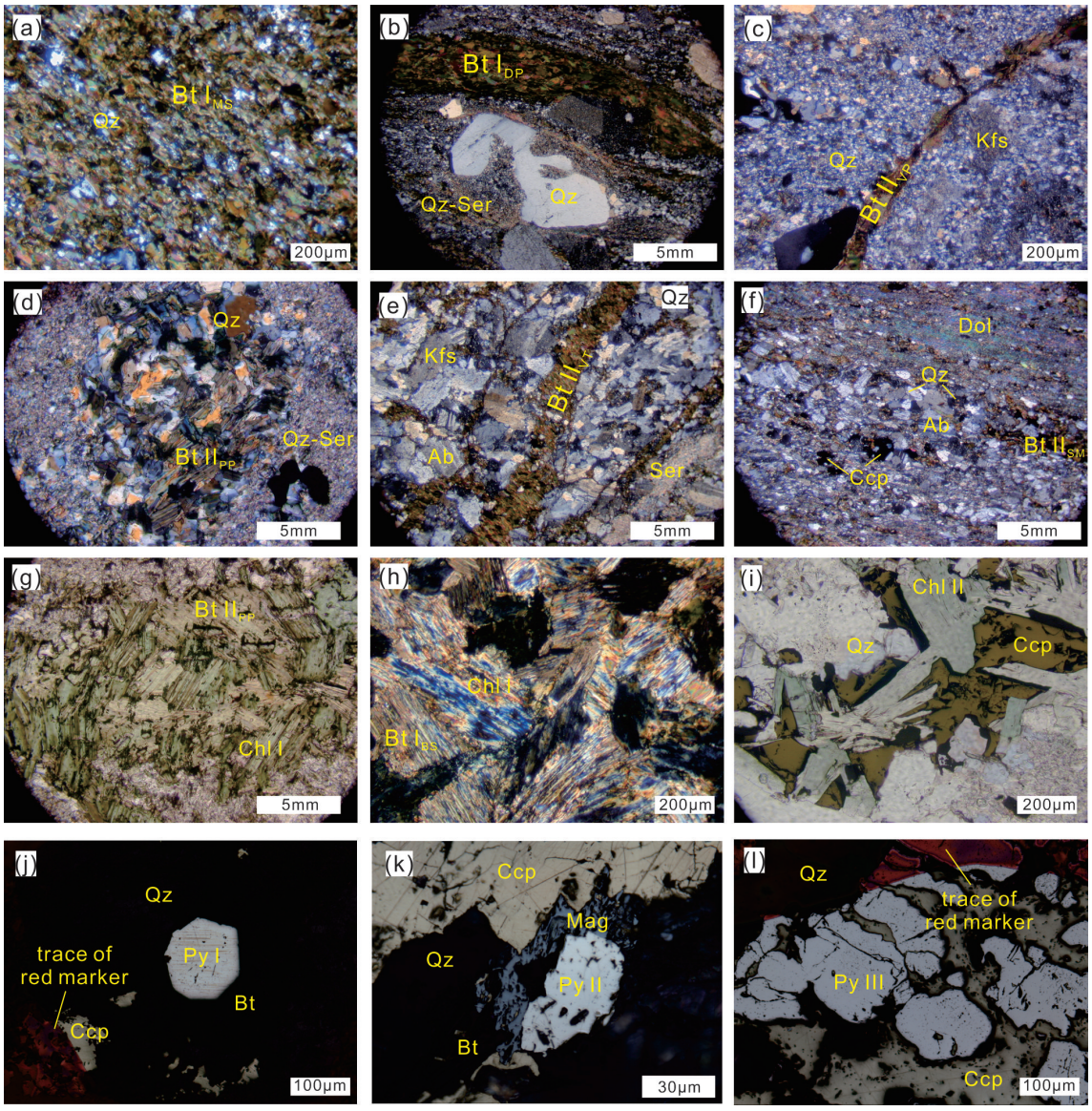

Figure 7. (**a**) Microscopic photos showing metamorphic biotite in biotite schist (Bt I_{BS}); (**b**) Biotite in monzogranite porphyry (Bt I_{DP}); (**c**) Biotite veins in monzogranite porphyry (Bt II_{VP}); (**d**) Secondary biotite replacing earlier phenocrystic biotite (Bt II_{PP}); (**e**) Biotite vein in metatuff (Bt II_{VT}); (**f**) Biotite growing with quartz-albite lenticulars in metatuff that overprinted by late vein-type chalcopyrite mineralization (Bt II_{SM}); (**g**) Chlorite replacing secondary biotite (Bt II_{PP}) in monzogranite porphyry; (**h**) Chlorite replacing biotite in biotite schist (Bt I_{BS}); (**i**) Chlorite growing with chalcopyrite in quartz vein; (**j**) Euhedral pyrite in metatuff (Py I); (**k**) Subhedral to anhedral pyrite intergrown with Bt II_{MT} in metatuff; and (**l**) subhedral to anhedral pyrite (Py III) in quartz veins. Ab; Albite; Bt: Biotite; Chl: Chlorite; Ccp: Chalcopyrite; Dol: Dolomite; Kfs: K-feldspar; Mag: Magnetite; Qz: Quartz; Ser: Sericite.

Based on the recently-revised Ti-in-biotite geothermometer [37] and assuming a pressure of 0.6 GPa, which was obtained for the Henglingguan mica schist and amphibolite by pseudosection thermobarometry and garnet-biotite-muscovite-aluminosilicate-quartz (GBMAQ) geobarometer [14], $\ln[T(°C)] = 6.313 + 0.224\ln(X_{Ti}) - 0.288\ln(X_{Fe}) - 0.449\ln(X_{Mg}) + 0.15P(GPa)$, where $X_j = j/(Fe + Mg + Al^{VI} + Ti)$, stage I biotite (Bt I_{BS} and Bt I_{DP}) has crystallization temperatures of 451 to 514 °C (averaging 474 ± 14 °C within 1σ), while stage II biotites have a temperature range of 439 to 549 °C (averaging 495 ± 19 °C within 1σ). These temperatures are close to the temperature estimates for post-peak metamorphism (545 ± 5 °C) and approximately 100 °C lower than the peak temperature (610 ± 20 °C) in the Henglingguan mica schist and amphibolite that were obtained

by garnet-biotite thermometers [14]. In terms of fugacities of volatiles, biotites in porphyry and mineralized veins have higher $\log(fH_2O)/(fHCl)$ (4.92 to 5.08) values than those in metatuff and schist have low $\log(fH_2O)/(fHCl)$ values (4.59 to 4.67). Based on a Fe^{3+} - Fe^{2+} - Mg^{2+} ternary diagram, all biotites plot above or adjacent to the HM buffer assemblage (hematite–magnetite) (Figure 8c). These estimates of oxygen fugacity is consistent with petrographic observations that biotite intergrow with hematite and magnetite in Stage II, and can even coexist with only hematite in the quartz biotite schist [10].

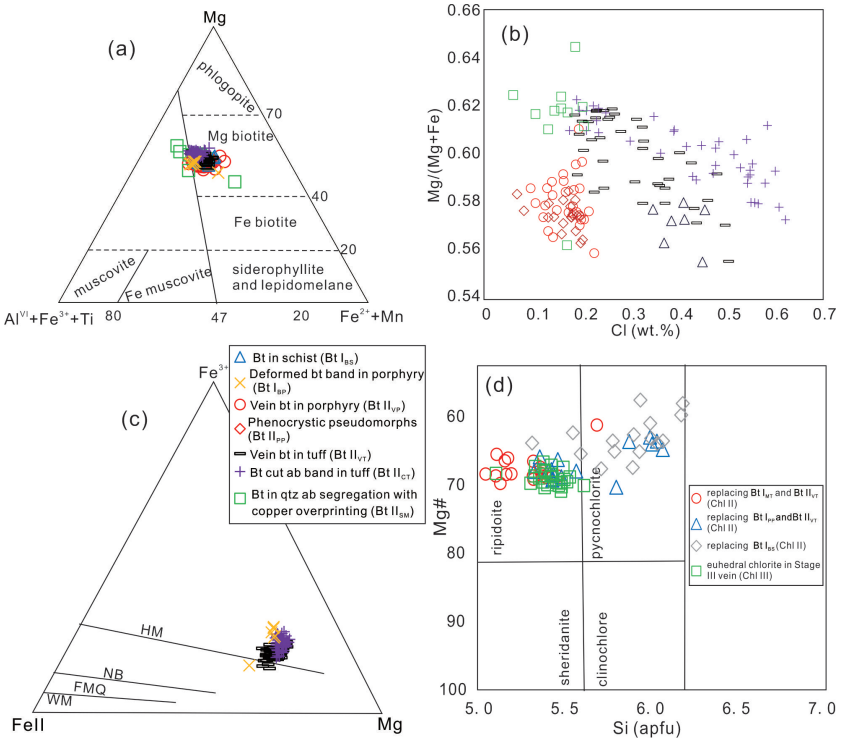

Figure 8. (**a**) Mg − (Al^{VI} + Fe^{3+} + Ti) − (Fe^{2+} + Mn) ternary diagram for biotite of the Tongkuangyu Cu deposit, North China Craton; (**b**) A Mg/(Mg + Fe) versus Cl plot for biotite; (**c**) Fe^{3+} - Fe^{2+} - Mg ternary diagram for oxygen fugacity estimation of biotite; (**d**) A plot of Mg♯ versus Si atoms for classification of chlorite at Tongkuangyu. MH: Magnetite-hematite buffer, NB: Nickel-bunsenite; FMQ: Fayalite-magnetite-quartz; WM: Wüstite-magnetite; Mg♯ = Mg/(Mg + Fe).

5.2.2. Chlorite

Chlorite of Tongkuangyu formed during the retrograde metamorphism and occurs as two forms, i.e., (1) as pseudomorphs replacing earlier biotite (Chl II) (Figure 7g,h), and (2) as euhedral grains in Stage III quartz vein (Chl III) (Figure 7i). A calculation on the basis of 28 oxygen atoms suggest that Chl II has a range of Si (5.05 to 6.18) and Mg/(Mg + Fe) values (0.55 to 0.69) while Chl III has consistent Si (4.72 to 5.61) and Mg♯ (0.64 to 0.69) (Table S2). On a Mg♯ versus Si classification diagram (Figure 8d), Chl II plots in a region overlapping ripidolite and pycnochlorite, and Chl III plots in the ripidolite field. Two different chlorite geothermometers yielded consistent results using the following calibrations: $T = -61.92 + 321.98 \times Al^{IV}$ [38], and $T = 319Al_c{}^{IV} - 69$ [39], where $Al_c{}^{IV} = Al^{IV} + 0.1(Fe/[Fe + Mg])$ Chl II has a temperature range from 230 °C to 410 °C (averaging 330 °C) and Chl III has temperatures of 320 °C to 465 °C (averaging 360 °C).

5.2.3. Sulfides

Pyrite of Tongkuangyu are categorized into three generations: The early euhedral pyrite (Py I), the intermediate-stage subhedral to anhedral pyrite (Py II) intergrowing with Bt II_{PP} and Bt II_{MT}, and the late subhedral to anhedral pyrite (Py III) intergrowing with chalcopyrite. Py I occurs in altered

porphyry and metatuff; Py II occurs only in altered porphyry; and Py III occurs in metatuff and quartz sulfide veins. Electron microprobe analyses (Table S3) revealed high and homogeneous Pb contents for all types of pyrite (0.12 to 0.49 wt.%, averaging 0.3 wt.%). Co and Ni concentrations in pyrite show strong dependence on host rock (Figure 9a). Pyrite in porphyry contains high contents of Ni (up to 0.14 wt.%) and low contents of Co (<0.03 wt.%). By contrast, pyrite in metatuff has low Ni but high Co, with euhedral ones containing a higher Co content (0.5 to 1.5 wt. %) than anhedral ones (0.2 wt. %). In addition, Py I in metatuff exhibits Co zonation, with a gradual increase from rims (0.5 to 1.0 wt.%) to cores (1.0 to 1.5 wt.%) (Figure 9b). Py III have intermediate contents of Co (0 to 0.6 wt.%) and Ni (0 to 0.05 wt.%). The other elements (Se, As, Te, Ni, Ag, Cu, and Au) are below the analytical detection limits. Chalcopyrite is one of the main copper bearing minerals. EPMA analyses indicate that chalcopyrite from the porphyry, biotite sericite quartz schist, and quartz sulfide vein are close to a pure composition except for high Pb contents (0.04 to 0.34 wt.%, averaging 0.21 wt.%) that are comparable to pyrite.

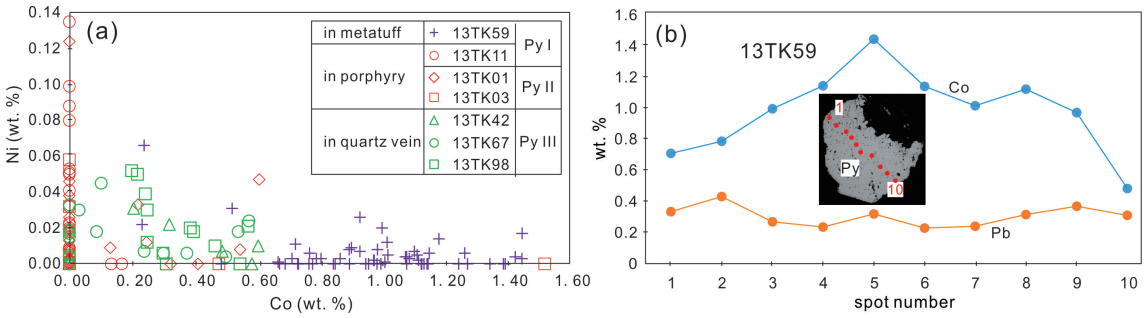

Figure 9. (**a**) A nickel versus cobalt plot for pyrite hosted in porphyry, metatuff, and quartz veins; (**b**) A diagram showing a profile of cobalt and lead concentration for an euhedral pyrite of metatuff (13TK59) from the Tongkuangyu Cu deposit, North China Craton; Note that euhedral pyrite exhibits gradual enrichment toward core and different pyrite exhibits different concentrations in the two elements.

Bornite in mica schist and quartz veins displays slight variations in Fe (7.3 to 12.0 wt.% and 11.4 to 11.7 wt.%), S (23.9 to 26.2 wt.% and 26.0 to 26.7 wt.%), and Cu (56.7 to 64.2 wt.% and 59.5 to 60.5 wt.%) contents. They have indistinguishable Pb (0.06 to 0.32 wt.%, averaging 0.17 wt.%) and Zn (0.04 wt.% to 0.09 wt.%, averaging 0.06 wt.%). All other elements are beyond the detection limits.

5.3. Stable Isotopes

5.3.1. H-O Isotopes

Xu et al. [6] reported that vein quartz has calculated $\delta^{18}O_{fluid}$ values of −123.3 to −40.8 ‰, and $\delta^{18}O_{fluid}$ values of 4.8 to 10.5 ‰, whereas quartz from disseminated ores displays calculated δD_{fluid} values of −30.2 to −84.9 ‰, and $\delta^{18}O_{fluid}$ values of 4.0 to 10.5‰ (Figure 10). These authors concluded that ore-forming fluids were from a mixed source with major components from magmatic waters.

In this study, biotite, chlorite, and quartz were investigated for hydrogen and oxygen isotopes. Biotite from porphyry, biotite schist, and metatuff had consistent δD (−66.5 ‰ to −97.8 ‰) and δ^{18}O (8.8 ‰ to 13.8 ‰) values (Table 3). Isotope equilibrium exchange equations [40,41], coupled with average Ti-in-biotite thermometric results (500 °C) indicate δD_{fluid} values of −28.4 ‰ to −59.4 ‰ and $\delta^{18}O_{fluid}$ values of 11.2 ‰ to 16.2 ‰. Similarly, chlorite from different lithologies also displayed consistent patterns, with δD between −68.5 ‰ and −68.9 ‰ and δ^{18}O values between 6.0 ‰ and 10.1 ‰ (Table 3). Using an Al-in-chlorite thermometric estimate (350 °C) and the isotopic equilibrium equations: $1000\ln\alpha\ Chl{-}H_2O = -22.4 \times (10^6/T^2) + 28.2 + (2X_{Al} - 4X_{Mg} - 68\times_{Fe})$ (for hydrogen isotopes between chlorite and waters, Suzuoki and Epstein [40]), where X is the molar fraction of the

cations; and 1000lnα Chl$-H_2O$ = 2.693 $\times$ ($10^9/T^3$) $-$ 6.342 $\times$ ($10^6/T^2$) + 2.969 $\times$ ($10^3/T$) (for oxygen isotopes between chlorite and waters, Cole and Ripley [42]), calculated δD_{fluid} (-18.9 to -29.3 per mil) and $\delta^{18}O_{fluid}$ values (6.4 ‰ to 10.5 ‰) suggesting less enrichment in deuterium but more enrichment in ^{18}O. Quartz from the early hematite-quartz vein and late magnetite - chalcopyrite - chlorite - quartz vein has consistent hydrogen (δD_{fluid} : -66.6 ‰ to -78.6 ‰) and oxygen ($\delta^{18}O_{qtz}$: 12.2 ‰ to 14.2 ‰) compositions according to the equation: 1000lnα Qtz$-H_2O$ = 3.38 $\times$ ($10^6/T^2$) $-$ 2.90 [43].

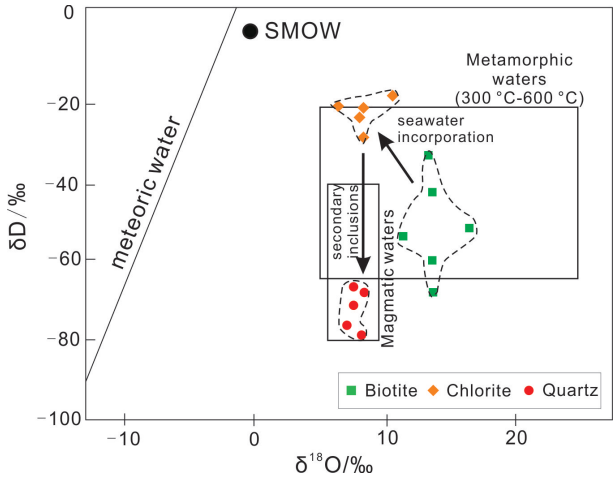

Figure 10. Hydrogen and oxygen isotope plot for biotite, chlorite, and quartz from the Tongkuangyu Cu deposit, North China Craton.

Calculated $\delta^{18}O_{fluid}$ values at 350 °C are 6.4 ‰ to 8.4 ‰ . On a $\delta D_{fluid} - \delta^{18}O_{fluid}$ diagram, biotite and chlorite plot in the field of metamorphic fluids whereas quartz plots in the magmatic water field. It should be noted that the quartz of biotite schist have similar $\delta^{18}O_{fluid}$ but much lower δD_{fluid} compared with biotite.

5.3.2. He-Ar Isotopes

A total of 5 sulfide separates from metatuff (13TK30, 13TK44) and vein-type mineralization (13TK62, 13TK67, and 13TK74) were analyzed for He and Ar isotopes in fluid inclusions. 13TK30, 13TK44, and 13TK67 are pyrite separates (a mixture of Py I and Py III) with purities >95 percent whereas 13TK62 and 13TK74 were dominated by chalcopyrite with minor amounts of pyrite (Py III). The sulfides showed no evidence of recrystallization and fluid inclusions in pyrite of several ore deposits revealed by near-infrared microscopy were mainly primary and pseudosecondary in origin [44–46]. Therefore, the released fluids likely derived from primary inclusions that precipitated the sulfides. Results show that fluids from the two generations have similar features. Both have high contents of radiogenic ^4He (24 $-$ 2850 $\times$ 10^{-7} ccSTP/g) and low contents of ^3He (0.8 $-$ 8.0 $\times$ 10^{-13} ccSTP/g), leading to crustal-like $^3He/^4He$ ratios of 0.002Ra to 0.023Ra (Ra: $^3He/^4He$ ratio of atmosphere of 1.384 $\times$ 10^{-6} ccSTP/g, Winckler et al. [47]) (Figure 11a; Table 4). Similarly, the fluids exhibit high radiogenic/excess $^{40}Ar^*$ (2.9 $-$ 9.0 $\times$ 10^{-7} ccSTP/g), but have low concentrations of ^{36}Ar (1.0 $-$ 1.8 $\times$ 10^{-10} ccSTP/g) and ^{38}Ar (0.16 $-$ 0.35 $\times$ 10^{-10} ccSTP/g). Air corrected $^{40}Ar/^{36}Ar$ ratios are very high (1723 $-$ 8623, averaging 4043). Corrected $^{38}Ar/^{36}Ar$ ratios are around 0.19 (Table 4). On a $^3He/^4He$ versus $^4He/\ ^{40}Ar^*$ plot, Tongkuangyu fluids contrast from mantle and magma-related fluids (such as porphyry copper deposit and intrusion-related gold deposit, Kendrick and Burnard [48]). Instead, their highly radiogenic nature resembles that of MVT deposits, which are commonly derived from crustal fluids [48] (Figure 11b).

Table 3. Hydrogen and oxygen isotopic composition of biotite, chlorite, and quartz of the Tongkuangyu Cu deposit, North China Craton.

Sample No.	Host Rock	Mineral	δD_{VSMOW} (‰)	$\delta^{18}O_{VSMOW}$ (‰)	$\delta^{18}O_{VSMOW}$ (‰)	$\delta D_{fluid,\ VSMOW}$ (‰)
13TK03	Porphyry	Biotite	−86.5	8.8	11.3	−54.0
13TK18	Hem two mica qtz schist	Biotite	−75.5	11.0	13.5	−43.0
13TK40	Biotite schist	Biotite	−66.5	10.9	13.4	−33.2
13TK51	Bt ser ab quartzite	Biotite	−97.8	11.0	13.6	−67.9
13TK53	Qtz ab sandstone cut by bt bands	Biotite	−85.6	13.8	16.3	−51.9
13TK55	Deformed porphyry	Biotite	−93.0	11.0	13.5	−60.0
13TK06	Qtz ser tuff	Chlorite	−58.5	10.1	10.5	−18.9
13TK07	Qtz two mica schist	Chlorite	−63.9	7.6	8.0	−24.3
13TK08	Qtz 2 mica schist	Chlorite	−61.5	7.9	8.3	−21.9
13TK85	Chl altered biotite schist	Chlorite	−61.1	6.0	6.4	−21.5
13TK94	Two mica schist	Chlorite	−68.9	7.9	8.3	−29.3
13TK30	Qtz breccia	Quartz	−78.6	14	8.2	
13TK44	Qtz breccia	Quartz	−68.0	14.2	8.4	
13TK62-1	Qtz vein	Quartz	−66.6	13.4	7.6	
13TK67	Qtz breccia	Quartz	−76.2	12.9	7.1	
13TK74	Qtz vein	Quartz	−71.2	13.4	7.6	

Table 4. Helium and argon isotopic compositions of sulfides of the Tongkuangyu Cu deposit, North China Craton. $^{40}Ar^*$: Excess ^{40}Ar content that is corrected for atmospheric argon

Sample No.	Host Rock	Mineral	Weight(g)	^{4}He (E^{-7} ccSTP/g)	^{3}He (E^{-7} ccSTP/g)	$^{3}He/^{4}He$ (Ra)	error	^{40}Ar (E^{-7} ccSTp/g)	^{36}Ar(E^{-7} ccSTP/g)	$^{40}Ar^*$ (E^{-7} ccSTp/g)	$^{40}Ar/^{36}Ar$	error	$^{38}Ar/^{36}Ar$	error
13TK30	Meta-tuff	Py	0.5	872.7	8.0E-06	0.010	0.001	4.6	0.00152	4.2	2780	49.8	0.189	0.003
13TK44	Sulfide vein	Py	0.9	381.3	7.8E-06	0.023	0.003	3.7	0.00084	3.4	4025	32.6	0.191	0.003
13TK62-1	Sulfide vein	Ccp	0.5	24.0	4.8E-07	0.023	0.002	9.3	0.00099	9.0	8623	195.5	0.187	0.003
13TK67	Sulfide vein	Py	0.5	150.2	7.9E-07	0.006	0.001	5.6	0.00167	5.1	3067	34.2	0.182	0.003
13TK74	Sulfide vein	Ccp	0.4	2849.6	5.8E-06	0.002	0.000	3.4	0.00183	2.9	1723	32.7	0.190	0.003

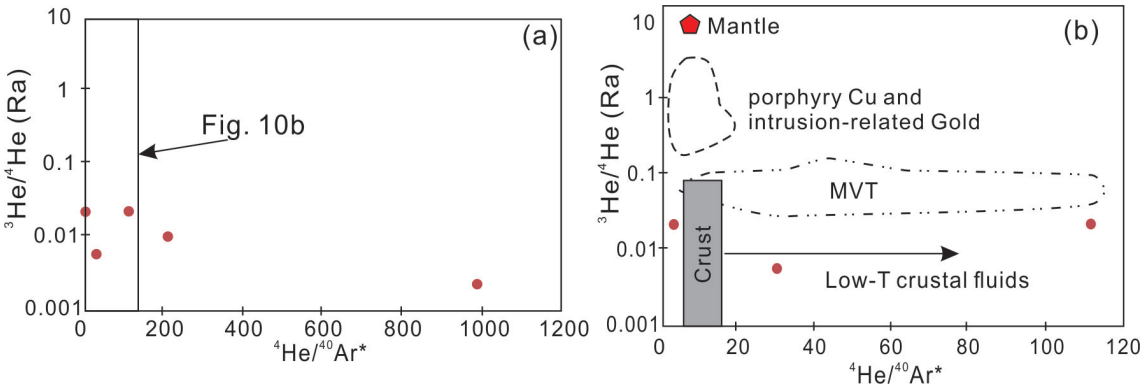

Figure 11. (**a**,**b**) ^{3}He/^{4}He versus ^{4}He/ ^{40}Ar* plots; Ra: ^{3}He/^{4}He ratio of atmosphere [47], ^{40}Ar*: Excess ^{40}Ar content that is corrected for atmospheric argon; data for Mantle, porphyry Cu, and intrusion-related Au, MVT deposits are from Kendrick and Burnard [48].

5.3.3. Sulfur Isotopes

Sulfur isotopes of sulfide have been intensively investigated by previous studies [5,6,49]. They discovered that disseminated sulfide (pyrite and chalcopyrite) displayed a δ^{34}S range from −4.5 ‰ to 6.8 ‰ and those from quartz veins had a δ^{34}S value range from −1.4‰ to 9.6 ‰. Results from this study generally agree with previous ones. Pyrites from metatuff and biotite schist have δ^{34}S values of 2.3 ‰ to 7.0 ‰, while one pyrite sample from a quartz vein had a δ^{34}S value of 3.1 ‰. Chalcopyrites from metatuff and quartz veins have a δ^{34}S range from 5.1 ‰ to 6.2 ‰. Bornites from porphyry and quartz veins have lower δ^{34}S values from 1.2 ‰ to 1.9 ‰ (Table 5).

Table 5. Sulfur isotopic composition of sulfides of the Tongkuangyu Cu deposit, North China Craton.

Sample No.	Host Rock	Mineral	δ^{34}S (‰)
13TK30	Metamorphosed tuff	Py	2.3
13TK67	Chalcopyrite quartz vein	Py	3.1
13TK89	Chalcopyrite quartz vein	Py	7
13TK44	Breciated quartz vein cemented by chalcopyrite	Ccp	4
13TK62-1	Breciated quartz vein cemented by chalcopyrite	Ccp	5.1
13TK74	Biotite schist with sulfide disseminates	Ccp	5.7
13TK90	Chalcopyrite quartz vein	Ccp	6.2
T04	Chalcopyrite quartz vein	Bn	1.2
TK11	Porphyry	Bn	1.9
TKYBN1	Breciated quartz vein cemented by chalcopyrite and bornite	Bn	1.5

6. Discussion

6.1. Timing of Copper Mineralization and its Relation to Metamorphism

The mineralization timing of Tongkuangyu was previously constrained by Re-Os dating of molybdenite. However, due to a poor understanding on the genetic relation between molybdenite and the main ore bodies, the meaning of these Re-Os ages remain unclear. Sulfide Pb-Pb isochron is considered a reliable method for dating ore deposits, especially for those containing highly radiogenic Pb [36]. Present and previous Pb isotopic analyses on sulfides from the entire Zhongtiao mountain district revealed extremely variable Pb isotopes, which form a tight linear array on a ^{207}Pb/^{204}Pb—^{206}Pb/^{204}Pb diagram. In theory, a Pb-Pb linear array can be interpreted in two ways, i.e., (1) as an isochron that derives from samples having the same initial Pb isotopic composition but different U/Pb ratios; and (2) as "errorchron" that is produced by mixing between high and low Pb ratio end-members. The latter model is not likely in this case for two reasons. Firstly, an end-member with a ^{206}Pb/^{204}Pb ratio up to 108 has not been discovered in this region, although the low-Pb end-member can be found such as the meta-porphyry and metatuff. Secondly, the poor correlation between the

$^{208}Pb/^{204}Pb$ and $^{207}Pb/^{204}Pb$ ratio (Figure 6b) requires special end-members that have heterogeneous thorogenic Pb in addition to homogeneous uranogenic Pb isotopic compositions. This essentially means that the end-members should possess variable U/Th ratios. No such rocks have been discovered in the Zhongtiao mountain. Considering this, we prefer to interpret the linear correlation as an isochron, and the isochron age of about 1.9 Ga is taken as the Cu mineralization timing of the Tongkuangyu and other copper deposits in the Zhongtiao mountain. This agrees with chalcopyrite Re-Os age of the Hujiayu deposit (1952 ± 39 Ma [13]) and molybdenite Re-Os age of the Tongmugou deposit (1901 ± 24 Ma [50]). In addition, although the exact initial Pb isotopic composition cannot be delineated due to unknown U/Pb ratios in the pyrite and chalcopyrite, the linear correlation indicates that all the copper deposits in the Zhongtiao mountain may have shared a common Pb source. Textural relationships suggest that the early conformable chalcopyrite intergrows with retrograde-metamorphic biotite (Figure 3a) and the late vein-type chalcopyrite replaces biotite (Figure 3m–o), indicating that they formed during retrograde metamorphism and after. This interpretation is consistent with the fact that the timing of metamorphism in the Zhongtiao mountain [14] as well as the Trans North China Orogen is around 1.9 Ga [51].

6.2. Origin of the Biotite and Chlorite

The origin of Tongkuangyu's biotite and chlorite remains hotly debated. Sun et al. [52] suggested that they are products of porphyry-style potassic and propylitic alterations. Other researchers infer that they are part of the pervasive metamorphic assemblages in the Zhongtiao mountain [5]. It has been well demonstrated that the chemical composition can be used to distinguish the biotite of different origins. By compiling 480 chemical data, Nachit et al. [53] constructed a FeO + MnO_2-MgO-TiO_2 diagram by studying biotite from various origins, which is capable of distinguishing between magmatic, neoformed (hydrothermal), and reequilibrated biotites. On the ternary diagram (Figure 12a), Tongkuangyu biotites plot in the field of reequilibrated biotite, which are dramatically different from magmatic and hydrothermal biotite, thus arguing against the porphyry model. In addition, on the FeO-Al_2O_3-MgO ternary diagram constructed by Gokhale [54] (Figure 12b), all the Tongkuangyu biotites plot in the field of metamorphic-metasomatic, which were originally represented by gneissis, schist, and meta-limestones. Evidently, Tongkuangyu biotite exhibits a geochemical affinity to metamorphic biotite. Above all, hydrogen-oxygen isotopic analyses show that the biotite-forming fluids at Tongkuangyu are enriched in both D and ^{18}O, and resemble metamorphic fluids and contrasts to magmatic fluids. Chlorite-forming fluids have δD and $\delta^{18}O$ values similar to metamorphic fluids although more enriched in heavy deuterium compared to biotite, likely indicating an involvement of D-rich fluids such as seawater during its crystallization. Through the above evidence, we suggest that biotite and chlorite of the Tongkuangyu deposit were largely formed by metamorphic fluids.

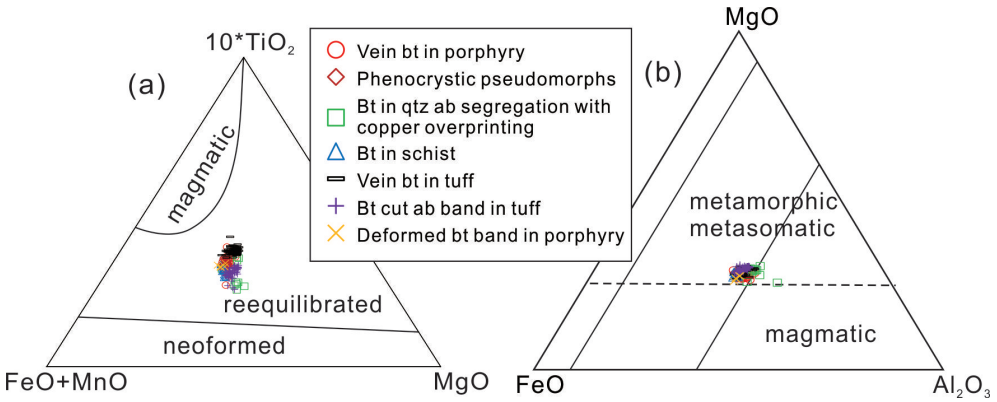

Figure 12. (**a**) A 10 × TiO_2-FeO + MnO-MgO ternary diagram from Nachit et al. [53]; (**b**) A MgO-FeO-Al_2O_3 ternary diagram from Gokhale [54].

6.3. Sources of Ore-Forming Fluids and Copper

The fluid source of the Tongkuangyu deposit was previously studied by hydrogen and oxygen isotopes in quartz [6,34]. Based on scattered data (δD_{fluid}:−30.2 to –123‰; $\delta^{18}O_{fluid}$: 3.98 to 10.5‰), the authors concluded that the fluids were of magmatic origin. Although quartz H-O isotope analyses from this study fall in the range of previous studies, biotite and chlorite H-O isotopic compositions argue strongly for a metamorphic origin. It has been shown that hydrogen isotopes in quartz are not a reliable indicator of fluid source due to the common presence of secondary fluid inclusions [55,56]. The prominent influence of secondary inclusions (normally meteoric water-dominant) is the suppression of the δD value. δD of biotite and chlorite are considered more reliable since they were directly measured on hydroxyl other than fluid inclusions. This explains why chlorite yielded higher δD_{fluid} values than the quartz at Tongkuangyu. Compared with the isotopic composition of biotite, the chlorite of Tongkuangyu contains less ^{18}O but more deuterium, indicating an involvement of ^{18}O-depleted and D-enriched fluids such as seawater. If this interference is correct, hydrothermal fluids may have primarily been metamorphic fluids involved for Stage II, and external fluids such as seawater were involved in Stage III.

This interpretation is supported by helium-argon isotopes of fluid inclusions in sulfide. The Tongkuangyu fluid is characterized by highly radiogenic helium ($^3He/^4He$: 0.002Ra to 0.023Ra) and argon (corrected $^{40}Ar/^{36}Ar$: 1723 *to* 8623) isotopes, which likely reflects either postentrapment modification or inheritance from fluid source. For He isotopic composition, preferential diffusion of ^3He out of the inclusion can decrease the $^3He/^4He$ ratio [48], but Hu et al. [57] demonstrate that this effect was a minor even at a 90 percent loss. In-situ production of ^4He and ^{40}Ar by radioactive elements such as U-Th-Sm and K may also modify the original isotopic compositions. However their daughter isotopes are normally bounded in the mineral lattice, which cannot be released by the analytical procedure of this study. Therefore, the $^3He/^4He$ ratios obtained are interpreted to be representative of the fluids trapped during sulfide precipitation. This feature rules out magmatic water which has high $^3He/^4He$ (6 to 9 Ra [47]), air-dominant meteoric water and seawater which have atmospheric He ($^3He/^4He$: 1Ra), and Ar ($^{40}Ar/^{36}Ar$: 295.5 [47]) signatures as a possible source. The He-Ar isotopes of the Tongkuangyu sulfides are close to crustal fluids ($^3He/^4He$: About 0.01 Ra [58]; $^{40}Ar/^{36}Ar$: n $\times$ 10^3 to n$\times 10^4$ [48]), especially those that interacted with crustal rocks containing radoactive elements such as U, Th, Sm, and K. At Tongkuangyu, the host rocks and underlying Archean basement are rich in radioactive elements and the breakdown of U-Th rich minerals and hornblende during prograde metamorphism may have provided sources of He and Ar [59,60]. The Tongkuangyu deposit has fairly variable $\delta D^{34}S$ values of -5 to 10 per mil. These values contrast markedly with the sedimentary $\delta^{34}S$ values of other deposits in this region (e.g., Hujiayu deposit: 10 to 22‰ [13]), and are considered as magmatic signatures [34]. However so far no 1.9 Ga magmatic activity has been discovered, and thus it is unlikely that the sulfur was supplied by an active magmatic-hydrothermal body. It is likely that the magmatic sulfides may have formed during the formation of host rocks at 2.2 Ga, and were remobilized by metamorphic fluids at 1.9 Ga. The remobilization of ore materials (S, Cu, Fe, etc.) from host rocks during metamorphism is supported by pyrite geochemistry. Pyrites in metatuff have high Co/Ni, whereas those in porphyry have low Co/Ni, possibly representing local remobilization of Co and Ni.

6.4. A Remobilization Model and Implication for Regional Metallogeny

New sulfide Pb-Pb dating and textural observation shows the copper mineralization at Tongkuangyu occurred during and post to retrograde metamorphism at ca. 1.9 Ga. Stable isotopes indicate a major contribution of metamorphic fluids during hydrothermal alteration and mineralization. These new data argue against any genetic interpretations relating Cu mineralization with magmatic-(such as porphyry) and sedimentary-hydrothermal processes. Nonetheless, molybdenite Re-Os age of ca. 2.1 Ga and sulfur isotopes with magmatic affinity might indicate the presence of precursor sulfide mineralizations before metamorphism. They likely formed in response to continental rifting volcanism

and sedimentation [10]. These preexisting mineralizations may have provided sources for subsequent copper remobilization. Therefore, we propose that, at ca. 2.2 Ga, initial stratabound copper sulfides may have been formed in response to either volcanism-related hydrothermal process or the circulation of external fluids in the copper-rich volcano-sedimentary rocks in the rift basin (Figure 13a).

At ca. 1.9 Ga (Figure 13b), the sulfide-bearing rocks underwent prograde metamorphism, which was possibly induced by continental collision between East and West blocks of the North China Craton [15]. The orogeny impacted all lithologies in the suture zone including Henglingguan and Zhongtiao formations. In the Zhongtiao mountain, index minerals such as staurolite, garnet, and scapolite formed at peak metamorphic conditions of 6.5 kbar and 610 °C, which was followed by retrogression. At depth, metamorphic fluids were released from the basement rocks as evidenced by He-Ar isotopic compositions. These fluids acquired high salinity most likely by dissolving the chlorine-rich scapolite as is supported by the dissolution textures (Figure 3h,i). The brines dissolved preexisting metal sulfides dissolution and obtained high Cu contents [61,62]. Subsequently, most of the ore materials were precipitated locally within weak zones, e.g., rock foliations and shear zones. The possible presence of early diagenetic iron oxides such as goethite prior to metamorphism buffered the oxidation state of the fluids to stabilize hematite, magnetite, and copper sulfides.

With further exhumation (Figure 13c), the ore-hosting terrane may have entered into a brittle deformation regime where faults and microcracks provided channels for fluid influx. External fluids that were preserved at higher crustal levels such as residue seawater and metamorphic fluids generated during prograde metamorphism could be pumped downward into the mineralization system through the brittle structures [63]. These fluids might have dissolved scapolite to acquire high salinity and sulfate radicals to form anhydrite daughter minerals in fluid inclusions in the mineralizing vein quartz [23]. The infiltration of the external fluids led to the evident increase in δD of the ore-forming fluids and remobilization of the earlier layered sulfides. Where the hybrid fluids were in contact with biotite, a redox reaction may have induced the precipitation of chalcopyrite and chlorite through the following reaction proposed for alteration of biotite under diagenetic conditions [64]:

$$\underset{\text{biotite}}{4KMgFe_2AlSi_3O_{10}(OH)_2} + 4SO_2 + 4H_2O + 2Cu^{2+} = \underset{\text{chlorite}}{2Mg_2Fe_3Al_2Si_3O_{10}(OH)_8} + \underset{\text{chalcopyrite}}{2CuFeS_2} + 6SiO_2 + 6O_2 + 4K^+$$

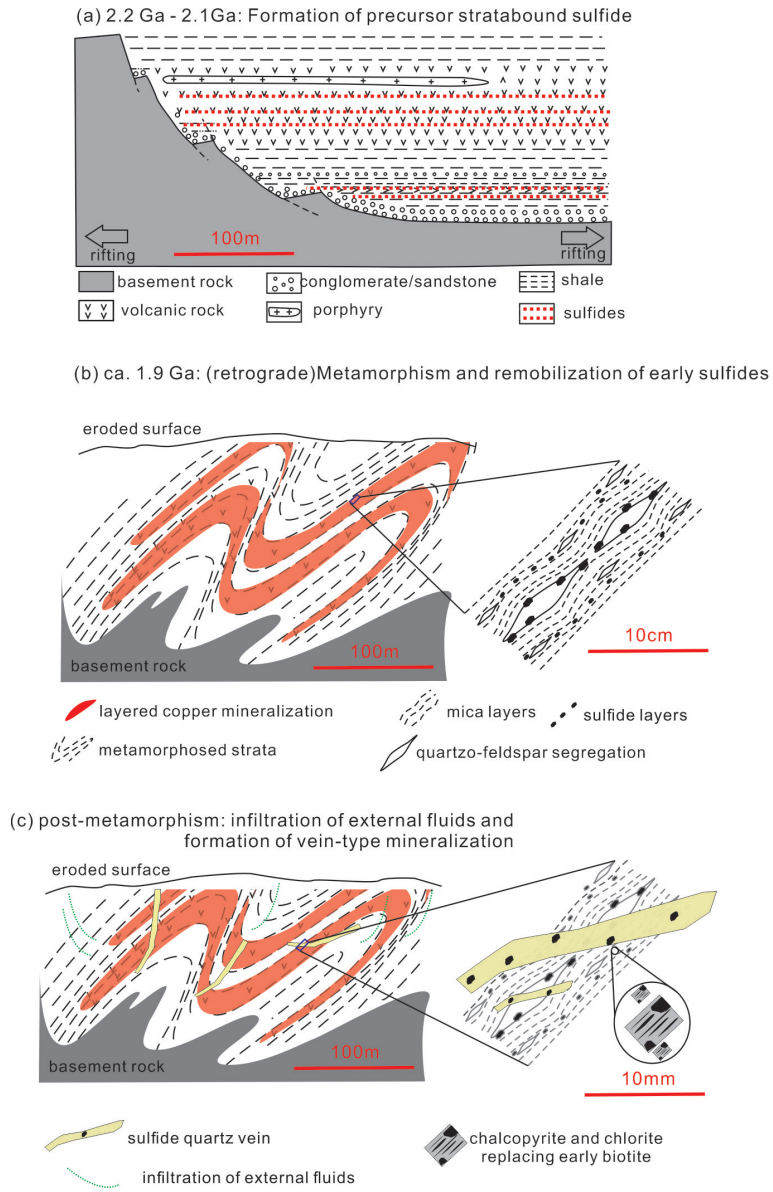

Figure 13. (**a**) A genetic model illustrating the formation of stratabound sulfide mineralizations during the development of a rift basin in the Tongkuangyu copper deposit at ca.2.2 to 2.1 Ga; (**b**) post to the peak metamorphism at ca.1.9 Ga, the precursor sulfides were remobilized by retrograde metamorphic fluids that generated by mineral breakup, and formed the layered mineralization and related mineral assemblage; and (**c**) with the further exhumation of the terrane, external fluids infiltrated into the metamorphic-hydrothermal system and formed quartz veins with a decreased oxygen fugacity and reduction reaction with early biotite.

7. Conclusions

Zircon U-Pb dating reveals that the ore-hosting metatuff of the Tongkuangyu Cu deposit were formed contemporaneous with other rocks at ca. 2180 Ma. Sulfide Pb-Pb isochron age of ca. 1960 Ma represent the formation age of the copper mineralization, corresponding to the timing of regional metamorphism. Geochemical and H-O isotopic analyses suggest that the biotite and chlorite were produced by metamorphic fluids rather than porphyry-style hydrothermal alterations. Thermobarometric estimations suggest that the biotite and chlorite were formed at ca. 500 °C and ca. 350 °C, respectively. Combined H-O and He-Ar isotopes suggest ore-forming fluids were derived from metamorphic fluids, and the late vein-type mineralization were formed with infiltration of external fluids. Sulfur isotopes and Co-Ni contents in sulfide indicate ore materials were likely derived from

the remobilization of preexisting sulfide in the host rocks. A two-stage metamorphic model involving remobilization of a precursor mineralization by metamorphic fluids and infiltration of external fluids was proposed.

Supplementary Materials: The following are available online at www.mdpi.com/xxx/s1, Table S1: Electron microprobe data for biotite of the Tongkuangyu copper deposit, Table S2: Electron microprobe data for chlorite of the Tongkuangyu copper deposit, Table S3: Electron microprobe data for sulfides of the Tongkuangyu copper deposit.

Author Contributions: Conceptualization, X.L.; Methodology, X.L., K.Y., and Z.Q.; Validation, B.R., F.H., and J.P.; Resources, B.R. and J.P.; Writing—original draft preparation, X.L.; Writing—review and editing, X.L., K.Y., B.R., Z.Q., F.H., and J.P.; Funding acquisition, X.L.

Funding: This research was supported by National Science Foundation of China (41402083, 41890833, 41602073) and China Scholarship Council (a visiting-scholar fellowship to XL).

Acknowledgments: Fei Su, Kuidong Zhao, Di Zhang, and Mu Liu are sincerely thanked for their assistance during zircon U-Pb, EPMA, and stable isotope analyses, respectively. Hongrui Fan and Fengchun Zhao are acknowledged for their great help during field work. An earlier version of this manuscript was greatly improved with the constructive and critical comments of Richard Palin. The manuscript benefited greatly from comments of three anonymous reviewers.

Conflicts of Interest: The authors declare no conflict of interest.

References

1. Sun, W.D.; Zhang, L.P.; Guo, J.; Li, C.Y.; Jiang, Y.H.; Zartman, R.E.; Zhang, Z.F. Origin of the mysterious Yin-Shang bronzes in China indicated by lead isotopes. *Sci. Rep.* **2016**, *6*, 23304. [CrossRef] [PubMed]
2. Wang, Z.; Wen, G. Zhongtiao mountain-style porphyry deposits. *Acta Geol. Sin.* **1957**, *37*, 401–415. (In Chinese with Russian Abstract)
3. Xie, J.R. Problems pertaining to geology and ore deposits of a copper deposits in Shansi province. *Sci. Sin.* **1963**, *12*, 1345–1356.
4. Sun, H.T.; Ge, C.H.; Ji, S.K. Tourmaline from the Zhongtiaoshan copper metallogenic area: Its characteristics and indication significance for ore-forming process of that area. *Acta Petrol. Miner.* **1989**, *8*, 232–242. (In Chinese with English Abstract)
5. CGGCDZM (Compilation group of the Geology of Copper Deposits of the Zhongtiao mountains). *Geology of Copper Deposits in the Zhongtiao Mountains*; Geological Publishing House: Beijing, China, 1978; pp. 1345–1356. (In Chinese)
6. Xu, W.X.; Guo, X.S.; Ji, S.K.; Lu, J.R.; Li, S.P. Geochemstry study of Tongkuangyu Cu deposit. *Miner. Resour. Geol.* **1995**, *9*, 77–86. (In Chinese)
7. Chen, W.M.; Li, S.P. Rhenium–osmium isotopic ages of sulfides from the Tongkuangyu porphyry copper deposit in the Zhongtiao mountain. *Miner. Depos.* **1998**, *17*, 224–228. (In Chinese with English Abstract)
8. Li, N.B.; Luo, Y.; Jiang, Y.H.; Guo, S.L.; Niu, H.C. Zircon U–Pb geochronology and Hf isotopic characteristic of metamorphic quartz-monzonite porphyry from Tongkuangyu area, Zhongtiao mountain and their geological implications. *Acta Petrol. Sin.* **2013**, *29*, 2416–2424. (In Chinese with English Abstract)
9. Jiang, Y.; Niu, H.; Bao, Z.; Li, N.; Shan, Q.; Yang, W. Fluid evolution of the Tongkuangyu porphyry copper deposit in the Zhongtiaoshan region: Evidence from fluid inclusions. *Ore Geol. Rev.* **2014**, *63*, 498–509. [CrossRef]
10. Liu, X.; Fan, H.R.; Santosh, M.; Yang, K.F.; Qiu, Z.J.; Hu, F.F.; Wen, B.J. Geological and geochronological constraints on the genesis of the giant Tongkuangyu Cu deposit (Palaeoproterozoic), North China Craton. *Int. Geol. Rev.* **2016**, *58*, 155–170. [CrossRef]
11. Liu, X.; Fan, H.R.; Yang, K.F.; Qiu, Z.J.; Hu, F.F.; Zhu, X.Y. Geochronology, redox-state and origin of the ore-hosting porphyry in the Tongkuangyu Cu deposit, North China Craton: Implications for metallogenesis and tectonic evolution. *Precambrian Res.* **2016**, *276*, 211–232. [CrossRef]
12. Qiu, Z.J.; Fan, H.R.; Liu, X.; Wen, B.J.; Hu, F.F.; Yang, K.F.; Guo, S.L.; Zhao, F.C. Fluid Inclusion and Carbon-Oxygen Isotope Studies of the Hujiayu Cu Deposit, Zhongtiao mountains, China: Implications for syn-metamorphic Copper Remobilization. *Acta Geol. Sin. Engl. Ed.* **2015**, *89*, 726–745. [CrossRef]

13. Qiu, Z.; Fan, H.; Liu, X.; Yang, K.; Hu, F.; Xu, W.; Wen, B. Mineralogy, chalcopyrite Re-Os geochronology and sulfur isotope of the Hujiayu Cu deposit in the Zhongtiao mountains, North China Craton: Implications for a Paleoproterozoic metamorphogenic copper mineralization. *Ore Geol. Rev.* **2016**, *78*, 252–267. [CrossRef]
14. Qiu, Z.; Fan, H.; Liu, X.; Yang, K.; Hu, F.; Cai, Y. Metamorphic PTt evolution of Paleoproterozoic schist-hosted Cu deposits in the Zhongtiao mountains, North China Craton: Retrograde ore formation during sluggish exhumation. *Precambrian Res.* **2017**, *300*, 59–77. [CrossRef]
15. Zhao, G.C.; Sun, M.; Wilde, S.A.; Li, S.Z. Late Archean to Paleoproterozoic evolution of the North China Craton: Key issues revisited. *Precambrian Res.* **2005**, *136*, 177–202. [CrossRef]
16. Xu, Q. Study on the Geological Characteristics and Ore Genesis of Tongkuangyu Copper Deposit in the Zhongtiaoshan Mountains, Shanxi Province. Master's Thesis, Jilin University, Changchun, China, 2010; p. 117. (In Chinese with English Abstract)
17. Sun, D.Z.; Li, H.M.; Lin, Y.X.; Zhou, H.F.; Zhao, F.Q.; Tang, M. Precambrian geochronology, chronotectonic framework and model of chronocrustal structure of the Zhongtiao mountains. *Acta Geol. Sin.* **1991**, *3*, 216–2316. (In Chinese with English Abstract)
18. Liu, X.; Fan, H.; Qiu, Z.; Yang, K.; Hu, F.; Wen, B. Formation ages of the Jiangxian and Zhongtiao groups in the Zhongtiao mountain region, North China Craton: Insights from SIMS U-Pb dating on zircons from intercalated plagioclase amphibolites. *Acta Petrol. Sin.* **2015**, *6*, 1564–1572. (In Chinese with English Abstract)
19. Zhao, F. Geochronologic and Geochemical Constraints on the Paleoproterozoic Crustal Evolution of Zhongtiao Mountains from Shanxi Province. Ph.D. Thesis, China University of Geosciences, Beijing, China, 2006; p. 172. (In Chinese with English Abstract)
20. Hu, W.; Sun, D. Mineralization and evolution of the early Proterozoic copper deposits in the Zhongtiao mountains. *Acta Geol. Sin.* **1987**, *2*, 152–165. (In Chinese with English Abstract)
21. Liu, C.; Zhao, G.; Sun, M.; Zhang, J.; Yin, C. U–Pb geochronology and Hf isotope geochemistry of detrital zircons from the Zhongtiao Complex: Constraints on the tectonic evolution of the Trans-North China Orogen. *Precambrian Res.* **2012**, *222–223*, 159–172. [CrossRef]
22. Liu, S.; Liu, C.; Li, Q.; Lü, Y.; Yu, S.; Tian, W.; Feng, Y. EPMA Th-U-Pb monazite dating of Zhongtiao and Lüliang Precambrian metamorphic complexes. *Front. Earth Sci.* **2007**, *14*, 64–74. (In Chinese with English Abstract) [CrossRef]
23. Jiang, Y.; Niu, H.; Bao, Z.; Li, N.; Shan, Q.; Yang, W.; Yan, S. Fluid evolution of the Paleoproterozoic Hujiayu copper deposit in the Zhongtiaoshan region: Evidence from fluid inclusions and carbon–oxygen isotopes. *Precambrian Res.* **2014**, *255*, 734–747. [CrossRef]
24. Zhao, Y.; Li, N.; Jiang, Y.; Niu, H.; Yang, W. Multi-stage Cu remobilization of the Huping metamorphic-hydrothermal deposit in the southern North China Craton. *Ore Geol. Rev.* **2018**, *101*, 870–884. [CrossRef]
25. Hu, Y. Mineralization and ore prognosis of the Tongkuangyu meta-porphyry copper deposit. *Miner. Depos.* **2000**, *19*, 46–53. (In Chinese with English Abstract)
26. Cui, C.X.; Zhen, Y.Q. Geology, alteration and metallogenesis of giant Tongkuangyu porphyry copper deposit in Zhongtiaoshan area. Contrib. *Geol. Miner. Resour. Res.* **2013**, *28*, 1–11. (In Chinese with English Abstract)
27. Wiedenbeck, M.; Alle, P.; Corfu, F.; Griffin, W.L.; Meier, M.; Oberli, F.; Quadt, A.V.; Roddick, J.C.; Spiegel, W. Three natural zircon standards for U-Th-Pb, Lu-Hf, trace element and REE analyses. *Geostand Geoanal. Res.* **1995**, *19*, 1–23. [CrossRef]
28. Sláma, J.; Košler, J.; Condon, D.J.; Crowley, J.L.; Gerdes, A.; Hanchar, J.M.; Whitehouse, M.J. Plešovice zircon-a new natural reference material for U-Pb and Hf isotopic microanalysis. *Chem. Geol.* **2008**, *249*, 1–356. [CrossRef]
29. Liu, Y.; Gao, S.; Hu, Z.; Gao, C.; Zong, K.; Wang, D. Continental and oceanic crust recycling-induced melt-peridotite interactions in the Trans-North China Orogen: U-Pb dating, Hf isotopes and trace elements in zircons of mantle xenoliths. *J. Petrol.* **2010**, *51*, 537–571. [CrossRef]
30. Ludwig, K.R. User's manual for Isoplot 3.00. A geochronological Toolkit for Microsoft Excel. *Berkeley Geochronol. Cent. Spec. Publ.* **2003**, *4*, 25–32.
31. He, H.; Zhu, R.; Saxton, J. Noble gas isotopes in corundum and peridotite xenoliths from the eastern North China Craton: Implication for comprehensive refertilization of lithospheric mantle. *Phys. Earth Planet. Inter.* **2011**, *189*, 185–191. [CrossRef]
32. Burnard, P.; Hu, R.Z.; Turner, G.; Bi, X.W. Mantle, crustal and atmospheric noble gases in ailaoshan gold deposits, Yunnan Province, China. *Geochim. Cosmochim. Acta* **1999**, *632*, 1595–1604. [CrossRef]

33. White, W.M. *Isotope Geochemistry*; John Wiley and Sons: Hoboken, NJ, USA, 2015; p. 492; ISBN 978-0470656709.
34. Xu, W.X.; Wang, L.M.; Li, H.; Guo, X.S. Isotope geochemistry of copper deposits in the Zhongtiao mountain. *Acta Geosci. Sin.* **2005**, *26*, 130–133. (In Chinese with English Abstract)
35. Sangster, D.F. Mississippi Valley-type and SEDEX lead-zinc deposits: A comparative examination. *Inst. Min. Metall. Trans. Sect. B Appl. Earth Sci.* **1990**, *99*, 21–42. [CrossRef]
36. Panneerselvam, K.; Macfarlane, A.W.; Salters, V.J. Reconnaissance Lead isotope characteristics of the Blackbird deposit: Implications for the age and origin of cobalt-copper mineralization in the Idaho Cobalt Belt, United States. *Econ. Geol.* **2012**, *107*, 1177–1188. [CrossRef]
37. Wu, C.; Chen, H. Revised Ti-in-biotite geothermometer for ilmenite-or rutile-bearing crustal metapelites. *Sci. Bull.* **2015**, *60*, 116–121. [CrossRef]
38. Cathelineau, M.; Izquierdo, G. Temperature-composition relationships of authigenic micaceous minerals in the Los Azufres geothermal system. *Contrib. Mineral. Petrol.* **1988**, *100*, 418–428. [CrossRef]
39. Jowett, E.C. Fitting iron and magnesium into the hydrothermal chlorite geothermometer. In Proceedings of the GAC/MAC/SEG Joint Annual Meeting, Toronto, ON, Canada, 27–29 May 1991; Program with Abstracts 16; Volume 16, p. A62.
40. Suzuoki, T.; Epstein, S. Hydrogen isotope fractionation between OH-bearing minerals and water. *Geochim. Cosmochim. Acta* **1976**, *40*, 1229–1240. [CrossRef]
41. Javoy, M. Stable isotopes and geothermometry. *J. Geol. Soc. Lond.* **1977**, *133*, 609–636. [CrossRef]
42. Cole, D.R.; Ripley, E.M. Oxygen isotope fractionation between chlorite and water from 170 to 350 ºC: A preliminary assessment based on partial exchange and fluid/rock experiments. *Geochim. Cosmochim. Acta* **1999**, *63*, 449–457. [CrossRef]
43. Clayton, R.N.; O'Neil, J.R. Mayeda TK. Oxygen isotope exchange between quartz and water. *J. Geophys. Res.* **1972**, *77*, 3057–3067. [CrossRef]
44. Kouzmanov, K.; Pettke, T.; Heinrich, C.A. Direct analysis of ore-precipitating fluids: Combined IR microscopy and LA-ICP-MS study of fluid inclusions in opaque ore minerals. *Econ. Geol.* **2010**, *105*, 351–373. [CrossRef]
45. Zhu, M.T.; Zhang, L.C.; Wu, G.; He, H.Y.; Cui, M.L. Fluid inclusions and He-Ar isotopes in pyrite from the Yinjiagou deposit in the southern margin of the North China Craton: A mantle connection for poly-metallic mineralization. *Chem. Geol.* **2013**, *351*, 1–14. [CrossRef]
46. Lüders, V. Contribution of infrared microscopy to studies of fluid inclusions hosted in some opaque ore minerals: Possibilities, limitations, and perspectives. *Mineral. Deposit.* **2017**, *52*, 663–673. [CrossRef]
47. Winckler, G.; Aeschbach-Hertig, W.; Kipfer, R.; Botz, R.; Rübel, A.P.; Bayer, R.; Stoffers, P. Constraints on origin and evolution of Red Sea brines from helium and argon isotopes. *Earth Planet. Sci. Lett.* **2001**, *184*, 184. [CrossRef]
48. Kendrick, M.A.; Burnard, P. Noble gases and halogens in fluid inclusions: A journey through the Earth's crust. In *The Noble Gases as Geochemical Tracers*; Springer: Berlin, Germany, 2013; pp. 319–369, ISBN 978–3-642-28835-7.
49. Sun, H.T.; Sun, J.G.; Xie, K.Q.; Yang, L.; Yin, W.D.; Xue, S.S. Ore-forming fluids and stable isotopes of the Tongkuangyu porphyry Cu deposit, Zhongtiao mountain. *Acta Geol. Sin.* **2015**, *89*, 151–153. (In Chinese)
50. Zhang, L.; Li, B.; Zhang, H.; Hu, A. Re-Os isotopic dating and its significance of molybdenite from the Tongmugou Cu deposit, Zhongitaoshan, Shanxi. *Glob. Geol.* **2013**, *32*, 740–7466. (In Chinese with English Abstract)
51. Qian, J.; Wei, C.; Zhou, X.; Zhang, Y. Metamorphic P–T paths and New Zircon U–Pb age data for garnet–mica schist from the Wutai group, North China Craton. *Precambrian Res.* **2013**, *2332*, 282–296. [CrossRef]
52. Sun, J.G.; Li, H.Y.; Liu, X.H.; Xie, K.Q.; Li, B.L.; Yin, D.W. Alteration and mineralization characteristics of Tongkuangyu copper deposit in Zhongtiao mountain, Shanxi Province. *Min. Depos.* **2014**, *33*, 1306–1324. (In Chinese with English Abstract)
53. Nachit, H.; Ibhi, A.; Abia, E.H.; Ohoud, M.B. Discrimination between primary magmatic biotites, reequilibrated biotites and neoformed biotites. *CR Geosci.* **2005**, *337*, 1415–1420. [CrossRef]
54. Gokhale, N.W. Chemical composition of biotites as a guide to ascertain the origin of granites. *Bull. Geol. Soc. Finl.* **1968**, *40*, 107–111. [CrossRef]
55. Goldfarb, R.J. Gold deposits in metamorphic rocks of Alaska. *Econ. Geol. Monogr.* **1997**, *9*, 151–190. [CrossRef]

56. Goldfarb, R.J.; Groves, D.I. Orogenic gold: Common or evolving fluid and metal sources through time. *Lithos* **2015**, *233*, 2–26. [CrossRef]
57. Hu, R.; Burnard, P.G.; Turner, G.; Bi, X. Helium and argon isotope systematics in fluid inclusions of Machangqing copper deposit in west Yunnan Province, China. *Chem. Geol.* **1998**, *146*, 55–63. [CrossRef]
58. Mamyrin, B.A.; Tolstikhin, I.N. *Helium Isotopes in Nature*; Elsevier: Amsterdam, The Netherlands, 1984; 273p, ISBN 9781483289809.
59. Palin, R.M.; White, R.W.; Green, E.C. Partial melting of metabasic rocks and the generation of tonalitic–trondhjemitic–granodioritic (TTG) crust in the Archaean: Constraints from phase equilibrium modelling. *Precambrian Res.* **2016**, *287*, 73–90. [CrossRef]
60. White, R.W.; Palin, R.M.; Green, E.C. High-grade metamorphism and partial melting in Archean composite grey gneiss complexes. *J. Metamorph. Geol.* **2017**, *12*, 1345–1356. [CrossRef]
61. Asadi, S.; Moore, F.; Fattahi, N. Fluid inclusion and stable isotope constraints on the genesis of the Jian copper deposit, Sanandaj–Sirjan metamorphic zone, Iran. *Geofluids* **2013**, *13*, 66–81. [CrossRef]
62. Heimann, A.; Spry, P.G.; Teale, G.S.; Leyh, W.R.; Conor, C.H.; Mora, G.; O'Brien, J.J. Geochemistry and genesis of low-grade metasediment-hosted Zn-Pb-Ag mineralization, southern Proterozoic Curnamona Province, Australia. *J. Geochem. Explor.* **2013**, *128*, 97–116. [CrossRef]
63. Yardley, B.; Gleeson, S.; Bruce, S.; Banks, D. Origin of retrograde fluids in metamorphic rocks. *J. Geochem. Explor.* **2000**, *69*, 281–285. [CrossRef]
64. Li, G.; Peacor, D.R.; Essene, E.J. The formation of sulfides during alteration of biotite to chlorite-corrensite. *Clay Clay Miner.* **1998**, *46*, 649–657. [CrossRef]